CMS analog front-end: simulations and measurements

Luigi Gaioni, for the BG/PV group

October 20, 2021

Contents

The analog front-end (FE) for the CMS pixel readout chip is based on the RD53A Linear FE, with improved comparator and threshold-tuning DAC. This brief report discusses the main features and settings of the CMS FE, and gathers a set of post-layout simulation results as obtained in different simulation corners.

1 FE description

The FE block diagram, with some transistor level details, is shown in figure 1. The readout chain includes a charge sensitive amplifier (CSA) with Krummenacher feedback complying with the expected large radiation induced increase in the detector leakage current and providing a linear discharge of the feedback capacitor C_F. The designed charge sensitivity, set by C_F, is around 26 mV/ke$^-$. The signal from the CSA is fed to a low power comparator that, combined with a time-over-threshold counter, is exploited for time-to-digital conversion. Channel to channel dispersion of the threshold is addressed by means of a local

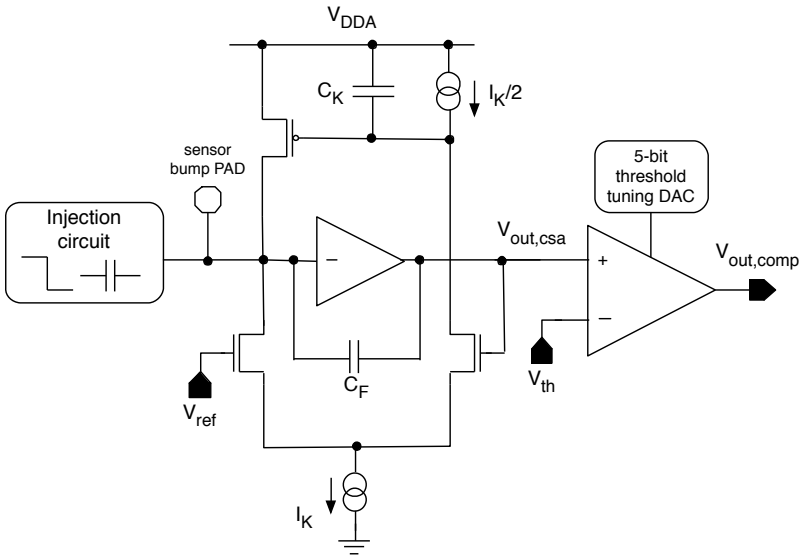

Figure 1: Schematic of the CMS analog front-end

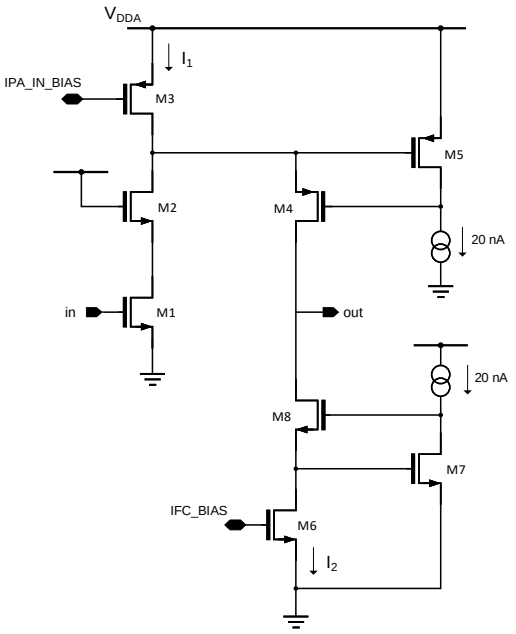

Figure 2: Charge sensitive amplifier forward gain stage.

circuit for threshold adjustment, based on a 5-bit, current-mode binary weighted DAC. The front-end chain has been optimized for a maximum input charge around 30000 electrons and features an overall current consumption close to 5 μA.

The core element of the charge sensitive amplifier is the gain stage shown in figure 2. This is a folded cascode architecture including two local feedback networks, composed by the M4-M5 and M7-M8 pairs, boosting the signal resistance seen at the output node. With a current flowing in the input branch equal to 3 μA and a current in the cascode branch close to 200 nA, the CSA is responsible for most of the power consumption in the analog front-end. The DC gain and the -3dB cutoff frequency of the open loop response, as obtained from simulations, are 76 dB and 140 kHz, respectively. The noise performance of the charge preamplifier is mainly determined by the contributions from the CSA input device and from the PMOS transistor part of the feedback network. The preamplifier gain

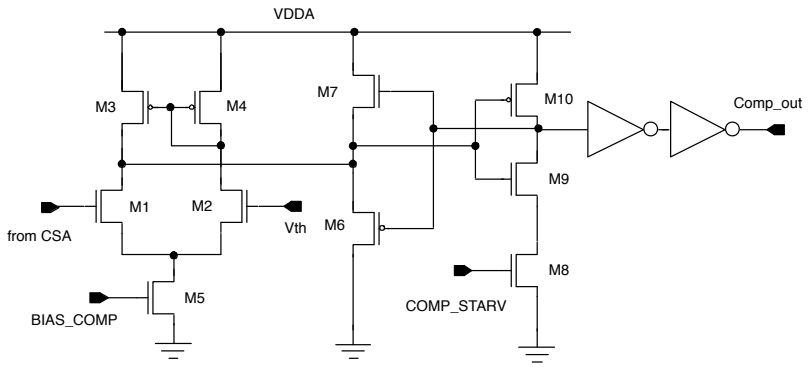

Figure 3: Threshold discriminator schematic diagram.

stage is identical to the one integrated in the RD53A Linear front-end. Notice that a gain selection bit was implemented in the RD53A version, whereas a single gain configuration is used in the CMS FE.
The comparator schematic diagram is shown in figure 3. It includes a transconductance stage (M1-M5) whose output current is fed to the input of a transimpedance (TIA) amplifier providing a low impedance path for fast switching. A couple of inverters is used

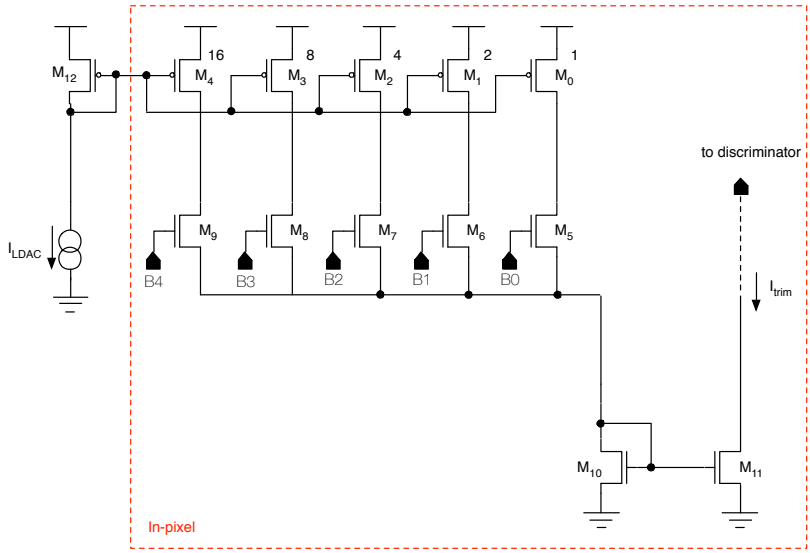

Figure 4: Threshold tuning DAC schematic diagram.

after the TIA in order to consolidate the logic levels. With respect to RD53A, the main modifications to the comparator are in its transimpedance stage. In particular, the TIA feedback network (transistors M6 and M7) has been modified with the aim of improving the time-walk performance of the front-end. A starving mechanism (transistor M8) has been added in the gain stage (M9 and M10) to limit the power consumption of the TIA. The trimming DAC schematic diagram is shown in figure 4. This is a 5-bit, current-mode, binary weighted DAC featuring regular current mirrors. The DAC output node, sinking a current I_{trim}, is connected to the output of the transimpedance stage of the comparator.

2 Front-end registers

Table 1 reports a list of the DAC settings for the CMS AFE, showing the recommended (Rec) values and the operating range (Std range). The recommended values are used to operate the front-end with a total analog current of 5 μA, with a Time-over-Threshold close to 130 ns for an input charge of 6000 electrons.

Table 1: Linear AFE settings

	Rec	Std Range
FC_BIAS_LIN	20	10-70
Vthreshold_LIN	-	REF_KRUM_LIN-900
COMP_LIN	110	70-250
COMP_STAR_LIN	110	50-300
LDAC_LIN	110	80-COMP_LIN×2
KRUM_CURR_LIN	70	5-200
PA_IN_BIAS_LIN	300	100-700
REF_KRUM_LIN	360	300-450

The DAC settings can be divided into two categories, in particular:

- Main settings:
  - Vthreshold_LIN
  - LDAC_LIN
  - KRUM_CURR_LIN
- Secondary settings
  - FC_BIAS_LIN

– COMP_LIN
– COMP_STAR_LIN
– PA_IN_BIAS_LIN
– REF_KRUM_LIN

The main DAC settings can be modified to achieve different threshold and ToT operation, whereas secondary settings should be in principle kept at their default value.

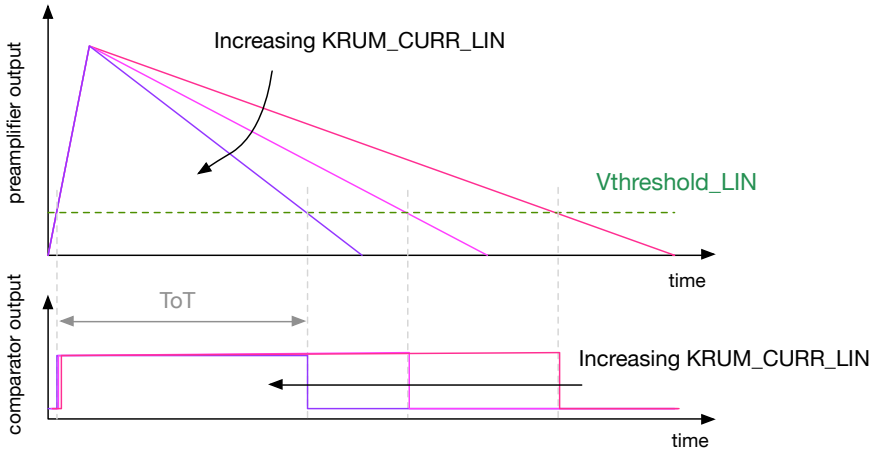

Figure 5: Effects of KRUM_CURR_LIN on preamplifier output waveform and ToT.

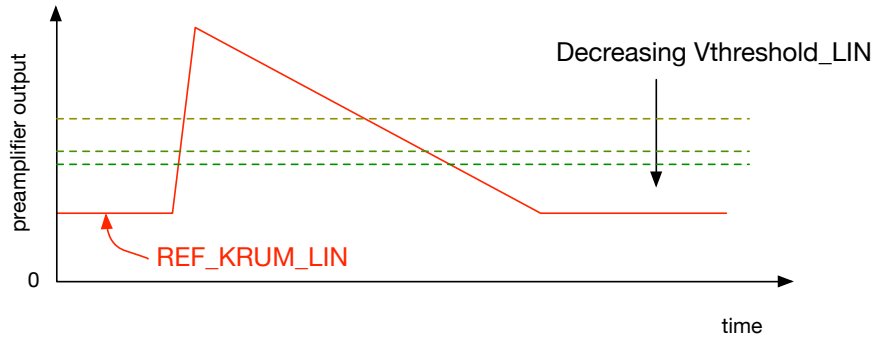

Figure 6: Effects of Vthreshold_LIN on the global threshold.

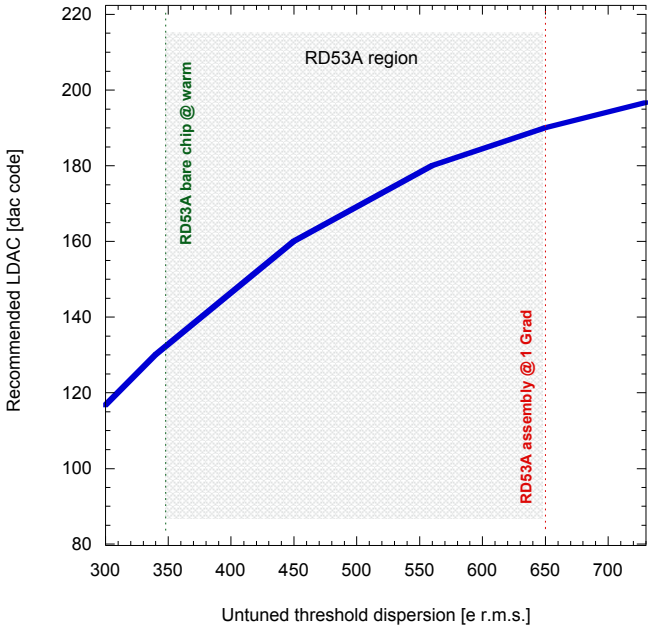

Figure 7: Recommended LDAC_LIN values as a function of the un-tuned threshold dispersion.

2.1 Krummenacher current: KRUM_CURR_LIN

KRUM_CURR_LIN sets the current in the Krummenacher feedback, used to linearly discharge the preamplifier feedback capacitance. Increasing KRUM_CURR_LIN results in a faster preamplifier return to baseline and a reduced Time Over Threshold (ToT), as schematically shown in Fig. 5. The recommended value, 70, should results in a ToT close to 133 ns for an input charge of 6000 electrons.

2.2 Global threshold: Vthreshold_LIN

Vthreshold_LIN sets the global threshold of the Linear AFE, corresponding to the DC threshold voltage applied to the discriminator input. Increasing Vthreshold_LIN results in an increased global threshold, as conceptually shown in Fig. 6. It is worth noticing that the effective threshold is the difference between Vthreshold_LIN and REF_KRUM_LIN which, in turn, sets the preamplifier output DC baseline (increasing REF_KRUM_LIN results in a higher baseline). Vhreshold_LIN=400 should provide a threshold (after tuning) close to 1000 electrons (as REF_KRUM_LIN is kept to 360).

2.3 Threshold trimming: LDAC_LIN

LDAC_LIN sets the LSB of the in-pixel threshold trimming DAC and, in turn, its output dynamic range. In particular, LDAC_LIN controls the current I_{LDAC} shown in the schematic of Fig. 4. Increasing LDAC_LIN results in increased LSB and output range. An increase in the un-tuned threshold dispersion is expected for the Linear AFE after irradiation. In that case it could be required to operate the front-end with an increased LDAC_LIN in order to compensate for the larger dispersion.
Recommended values of LDAC_LIN are shown in Fig. 7 as a function of the un-tuned threshold dispersion. Typical values of the untuned threshold dispersion before irradiation are in the range 350-550 electrons (as obtained from RD53A and prototype measurements, depending on sensors geometry, temperature, ...). As shown in the figure, the untuned threshold dispersion can get up to 650 electrons after irradiation at 1 Grad (from RD53A measurements).

2.4 Secondary settings

The DAC settings listed in this section are mainly related to preamplifier and comparator bias and should be, in principle, kept at their default value. A brief overview of these settings is given in the following.

- FC_BIAS_LIN: sets the current in the preamplifier folded cascode branch.
- COMP_LIN: sets the bias current in the threshold discriminator input (transconductance) stage. This parameter can be slightly increased to improve speed.
- COMP_STAR_LIN: sets the maximum current flowing in the comparator output branch (controlled by the starving transistor M8 in Fig. 3).
- PA_IN_BIAS_LIN: sets the current in the preamplifier input branch. This current represents the main contribution to the Linear AFE current consumption. This parameter can be slightly decreased to reduce power, at the cost of an increased noise.
- REF_KRUM_LIN: as explained in section 2.2, this parameter sets the preamplifier output DC baseline ($V_{out,csa}$ in Fig. 1).

3 Post-layout simulation results

A number of post-layout simulations have been performed on the CMS FE in different corners, shown in Tab. 2-4. The FE analog current has been tuned to 5 μA for the Typ OP corner and for the 500Mrad TT corners, without retuning of other parameters.

Table 2: Pre-rad corners

	Typ RO	**Typ OP**	**FS OP**	**SF OP**	**SS OP**	**FF OP**	**SS LT**	**FF LT**
Model	TT	TT	FS	SF	SS	FF	SS	FF
VDD	1.2	1.2	1.08	1.08	1.08	1.32	1.08	1.32
T	27	-30	-30	-30	-30	-30	-40	-40

Table 3: 500 Mrad corners, -30°C

	500 Mrad	**500 Mrad**	**500 Mrad**	**500 Mrad**	**500 Mrad**	**500 Mrad**	**500 Mrad**
Model	TT	FS	SF	FF	FF	SS	SS
VDD	1.2	1.2	1.2	1.2	1.32	1.2	1.08
T	-30	-30	-30	-30	-30	-30	-30

Table 4: 500 Mrad corners, 0°C

	500 Mrad	**500 Mrad**	**500 Mrad**	**500 Mrad**	**500 Mrad**	**500 Mrad**	**500 Mrad**
Model	TT	FS	SF	FF	FF	SS	SS
VDD	1.2	1.2	1.2	1.2	1.32	1.2	1.08
T	0	0	0	0	0	0	0

The threshold has been set to 1000 electrons in each corner. A brief discussion of the simulations results is provided in the following sections.

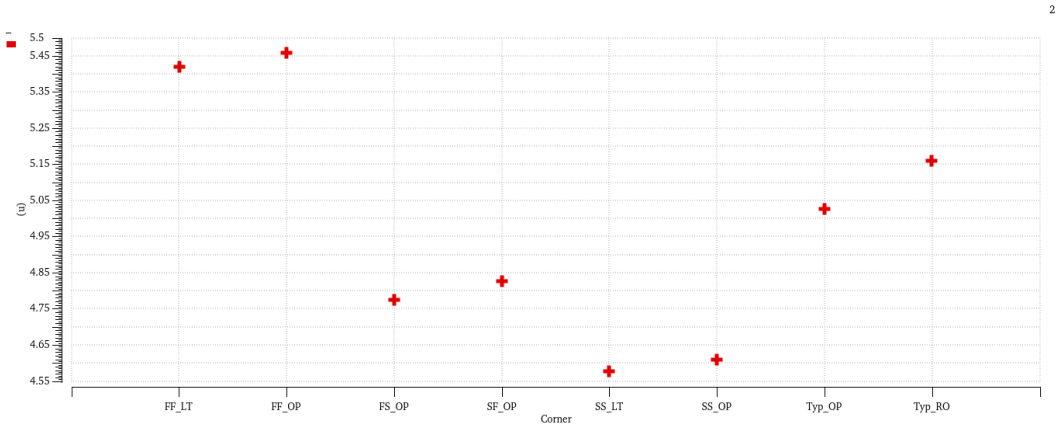

Figure 8: Analog power supply current in the different corners.

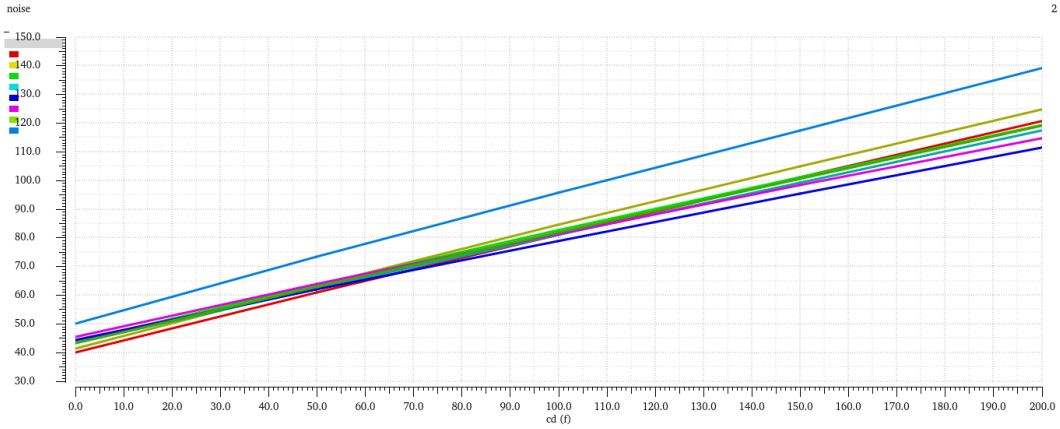

Figure 9: Equivalent noise charge as a function of the detector capacitance.

3.1 Pre-rad results

3.1.1 Power supply current, noise and charge sensitivity

Fig. 8 shows the total analog current drawn by the single pixel. As mentioned, the FE has been tuned to 5 μA in the Typ OP corner. The plot reveals a maximum current in the FF OP corner (5.5 μA) ad a minimum in the SS LT corner (4.6 μA).
Fig. 9 shows the Equivalent Noise Charge (ENC) as a function of the detector capacitor C_D for the simulated corners, for C_D ranging from 0 to 200 fF. An ENC around 60 electrons has been obtained in the Typ OP corner for a detector capacitance of 50 fF. The higher

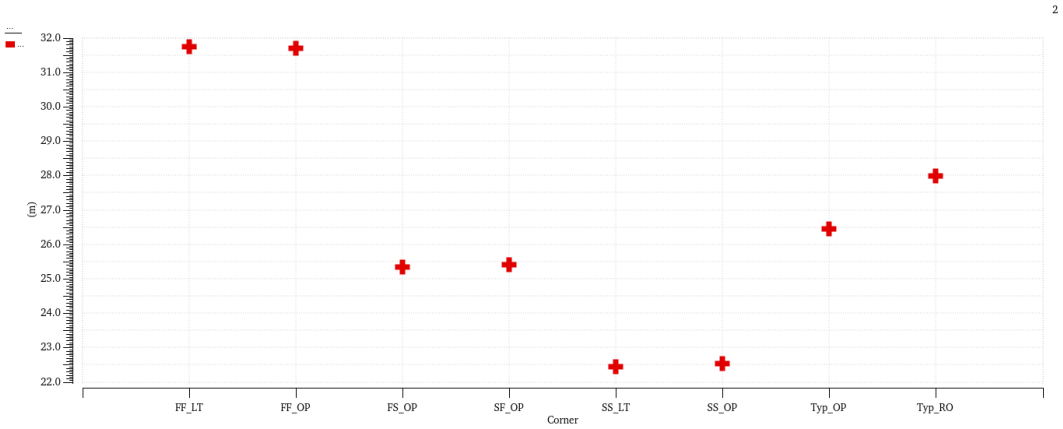

Figure 10: Preamp charge sensitivity G_q for the simulated corners.

values of the ENC (cyan curve) are relevant to the FF OP corner, for which a 25% larger noise has been detected at C_D=50 fF.
Fig. 10 shows the CSA charge sensitivity, G_q (in mV/ke$^-$), in the different corners. A G_q around 26 mV/ke$^-$ has been obtained in the Typ OP corner, with ±20% variations in the simulated corners. Main contributions to the charge sensitivity fluctuations are the variations of the CSA feedback capacitor and of the Krummenacher feedback current (not tuned in the different corners).

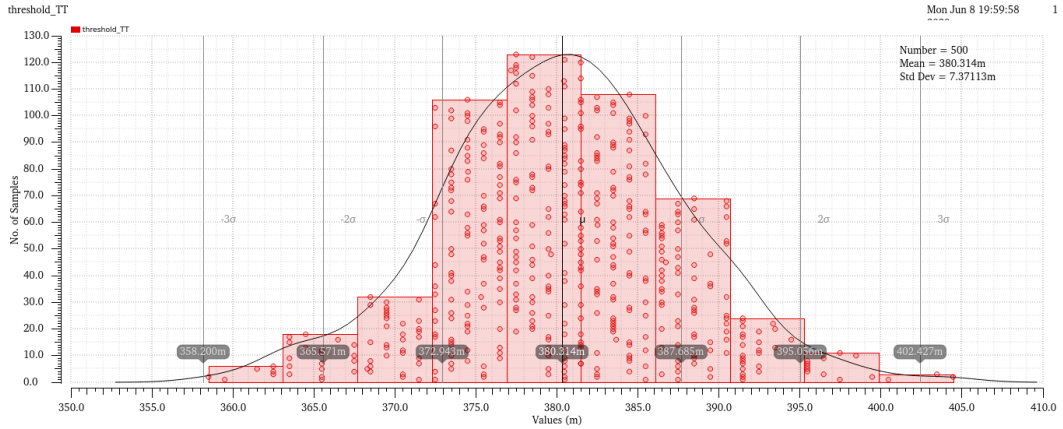

Figure 11: Un-tuned threshold distribution for the Typ OP corner. Threshold is evaluated at the comparator input (in mV).

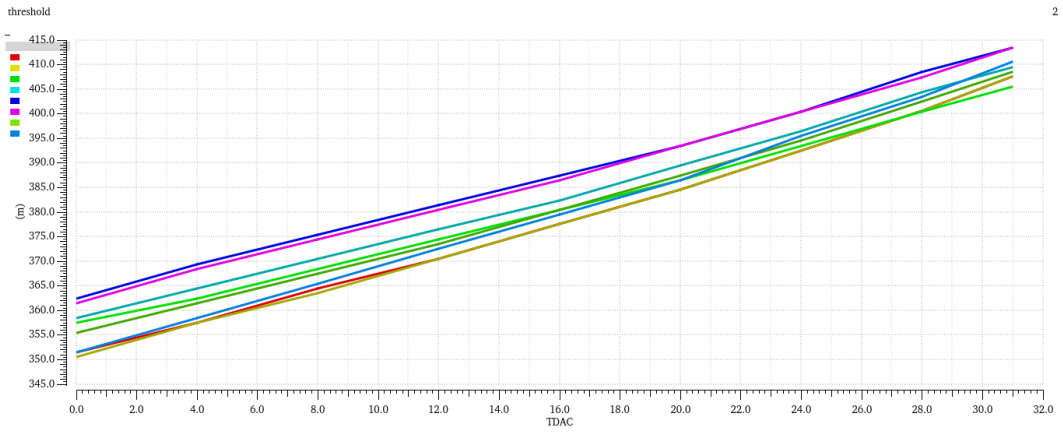

Figure 12: Comparator effective threshold (in mV) as a function of the TDAC code, for LDAC_LIN=140.

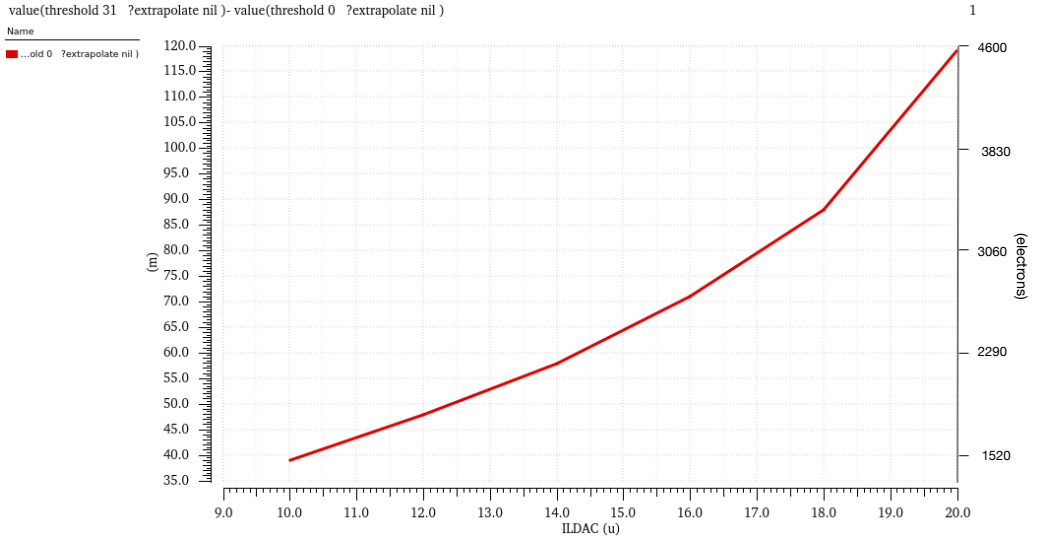

Figure 13: TDAC dynamic range, in mV, as a function of ILDAC current, controlled by LDAC_LIN register. LDAC_LIN=10×ILDAC.

3.1.2 Threshold dispersion and TDAC range

Fig. 11 shows the threshold distribution for the Typ OP corner. Threshold is evaluated at the comparator input, in mV, by means of DC sweeps of the global threshold. The distribu-

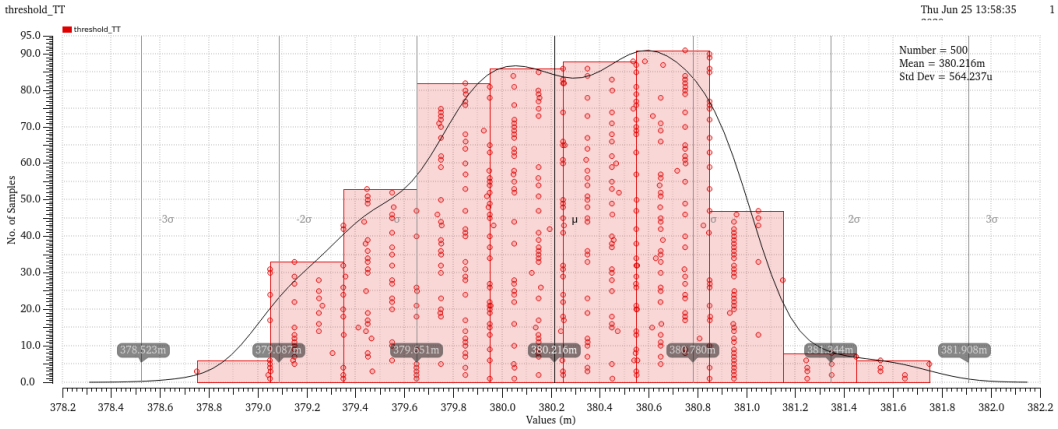

Figure 14: Tuned threshold distribution for the Typ OP corner. Threshold is evaluated at the comparator input (in mV).

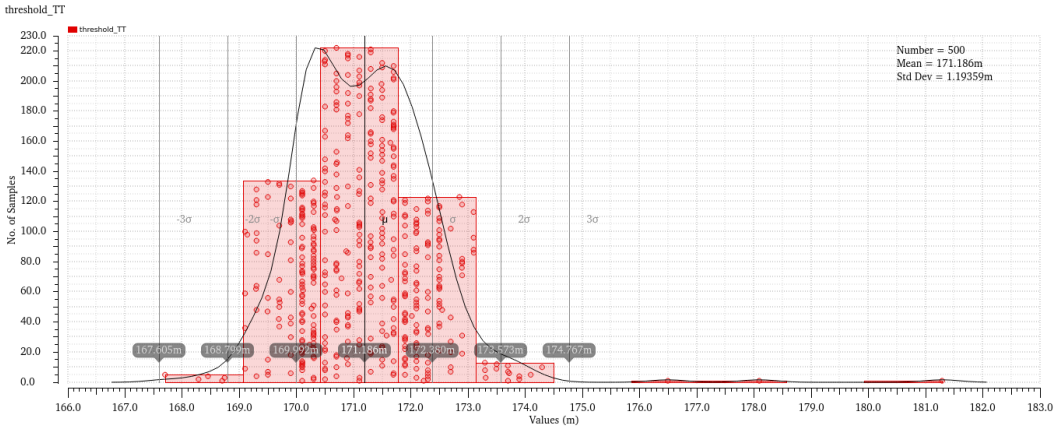

Figure 15: Tuned threshold distribution for the Typ OP corner with an additional source of threshold dispersion. Un-tuned threshold dispersion close to 750 electrons. Tuned dispersion, around 1.2 mV from the distribution fitting, corresponds to 46 electrons.

tion features a standard deviation, σ_{Vth}, of 7.4 mV, which can be converted into electrons by dividing by the CSA charge sensitivity G_q, resulting in an un-tuned threshold dispersion, σ_{Qth}, around 300 electrons. From circuit simulations a TDAC dynamic range around 45 mV ($6 \times \sigma_{Vth}$) is thus required in order to compensate for the threshold dispersion. It has to be noticed that the measured un-tuned threshold dispersion on RD53A samples of the Linear FE is in general larger than simulated values, and depends on different factors

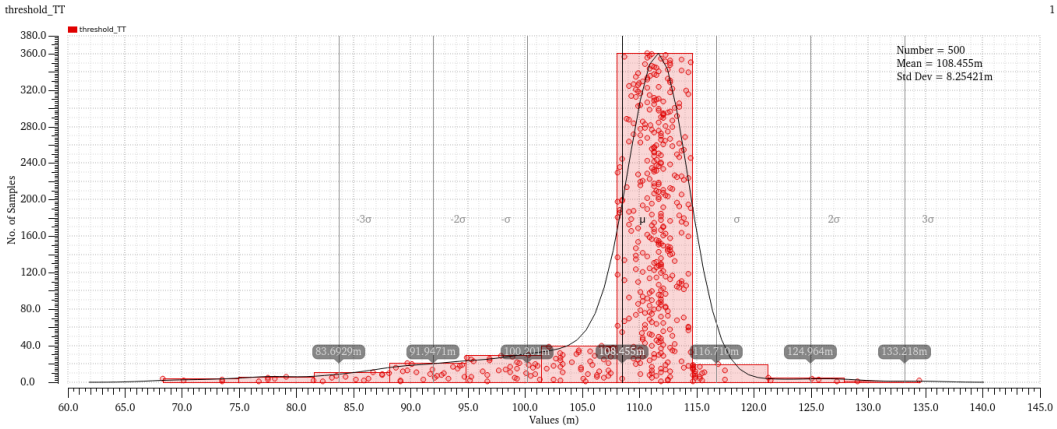

Figure 16: Tuned threshold distribution for the RD53A Linear front-end with an additional source of threshold dispersion. Un-tuned threshold dispersion close to 750 electrons. Tuned dispersion, around 8.2 mV, corresponds to a dispersion larger than 300 electrons. Large tails in the distribution.

such as radiation, temperature and sensor type. For this reason, in the actual chip, the TDAC dyanmic range should be adjusted according to results shown in Fig. fig:LDAC.
Fig. 12 shows the effective threshold (evaluated, in mV, at the comparator input) as a function of the TDAC code, for LDAC_LIN set to 140. For the different corners, a TDAC dynamic range (i.e. the difference between threshold at TDAC=31 and the one obtained at TDAC=0) around 60 mV has been obtained. Again, it is possible to translate this value in electrons at the FE input by dividing by G_q, resulting in a dynamic range close to 2300 electrons. The TDAC dyanmic range as a function of the ILDAC current, controlled by the LDAC_LIN register, is shown in Fig. 13. Notice, from Table 1, that the maximum LDAC_LIN should not exceed 2 $\times$ COMP_LIN: if this happens, the maximum current generated by the TDAC (for higher TDAC codes) gets larger than the maximum output current of the transconductor integrated in the threshold discriminator, resulting in a non-optimal behaviour of the front-end. It can be noticed that the maximum achievable dynamic range is 120 mV, corresponding to a range of 4600 electrons.
An Ocean script has been developed in order to simulate the tuned threshold dispersion of the CMS FE. Fig. 14 shows the threshold distribution after trimming for the Typ OP corner. Notice that the standard deviation of the distribution, around 560 μV, is reduced by a factor of 13 with respect to the pre-tuning value.
Since, in general, the simulated threshold dispersion is smaller than the one measured on RD53A chips, a simulation with an additional source of dispersion has been carried out to verify the front-end behavior at very high levels of un-tuned threshold dispersion. In particular it has been studied the maximum un-tuned threshold dispersion that the FE can

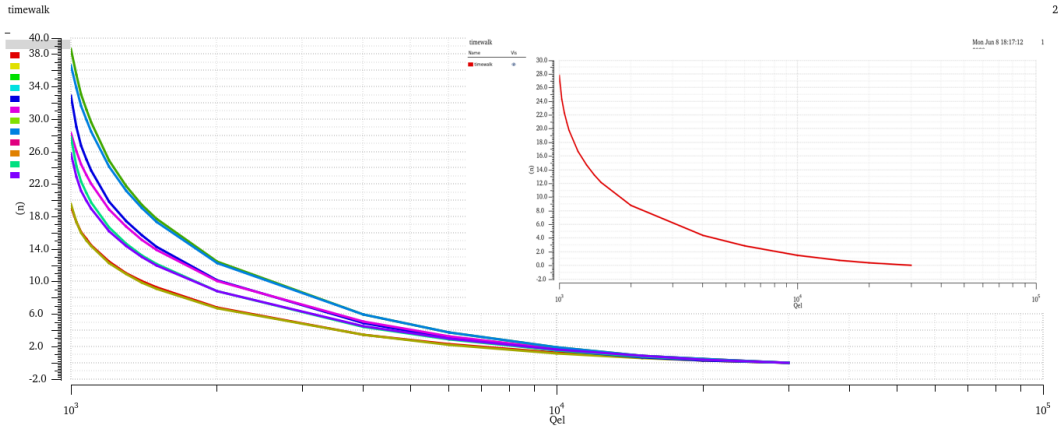

Figure 17: Time-walk as a function of the input charge (log-scale x-axes). The inset shows the results for the Typ OP corner.

afford with a fraction of non-tunable pixels smaller than 1%. Fig 15 shows the threshold distribution obtained after trimming with an un-tuned dispersion of 750 electrons. This simulations show that 99.4% of the pixels can be tuned (notice 3 outlier pixels over 500 runs of a Monte-Carlo simulation), with a tuned threshold dispersion close to 1.2 mV, corresponding to 46 electrons. For the sake of the comparison, Fig. 16 shows the result for the same simulation carried out on the RD53A Linear front-end. Tuning does not work properly for the RD53A version, as pointed out by the large threshold dispersion after tuning (8.25 mV, corresponding to a dispersion larger than 300 electrons) and the very large tails in the distribution.

3.1.3 Timewalk and Time-over-Threshold

Fig. 17 shows the time-walk as a function of the input charge, for signals ranging from 1000 to 30000 electrons (log-scale on x-axes). The inset shows the time-walk for the Typ OP corner, featuring 28 ns time-walk for an input charge equal to the threshold. An input charge close to 1020 electrons is needed to achieve 25 ns time-walk, resulting in an in-time overdrive around 20 electrons. The worst-case corner is the SS LT, with a time-walk around 38 ns for an input charge close to the threshold.
Fig. 18 shows the Time-over-Threshold (ToT) for input charge signals ranging from 1000 to 30000 electrons (lin-scale on x-axes). As for the RD53A Linear front-end, a good linearity for signals larger than 2000 electrons is achieved.
Fig. 19 shows the ToT distribution for an input charge of 6000 electrons, obtained after threshold trimming by means of 500 runs of a Monte-Carlo simulation. The mean ToT value, with KRUM_CURR_LIN register set to 70, is close to 126 ns with a standard de-

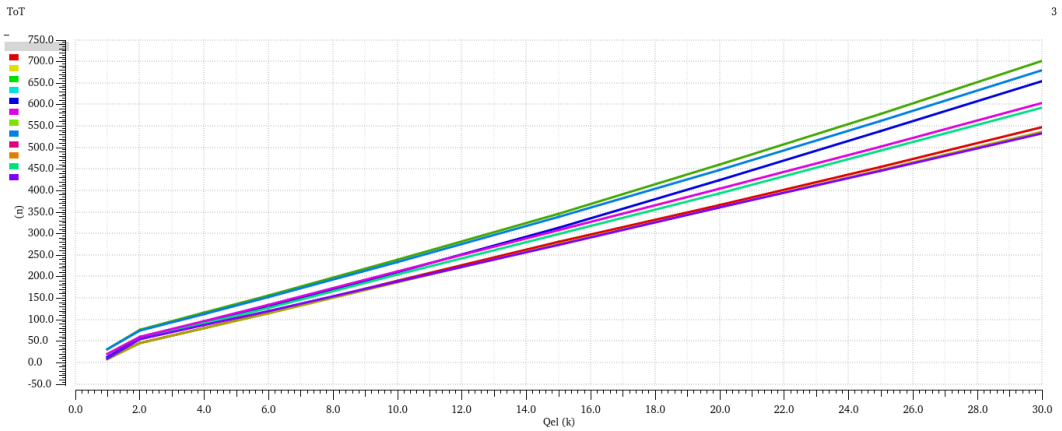

Figure 18: Time-over-Threshold as a function of the input charge (lin-scale x-axes).

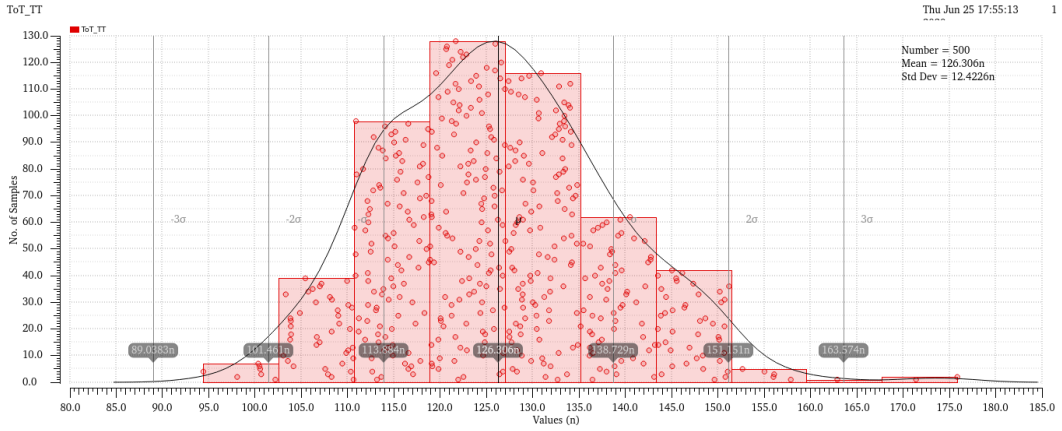

Figure 19: ToT distribution for an input charge of 6000 electrons. Data obtained after threshold trimming.

viation of 12.4 ns. A slightly larger ToT dispersion is obtained with the un-tuned matrix (16.4 ns). A very small time dispersion of the hit leading edge signal has been obtained, as shown in Fig. 20, which shows the time distribution of the hit signal for an input charge of 6000 electrons (notice the small standard deviation). Nonetheless, as the input charge is reduced, the dispersion increases significantly, as shown in Fig. 21, reporting the hit timing distribution for an input charge of 1200 electrons.

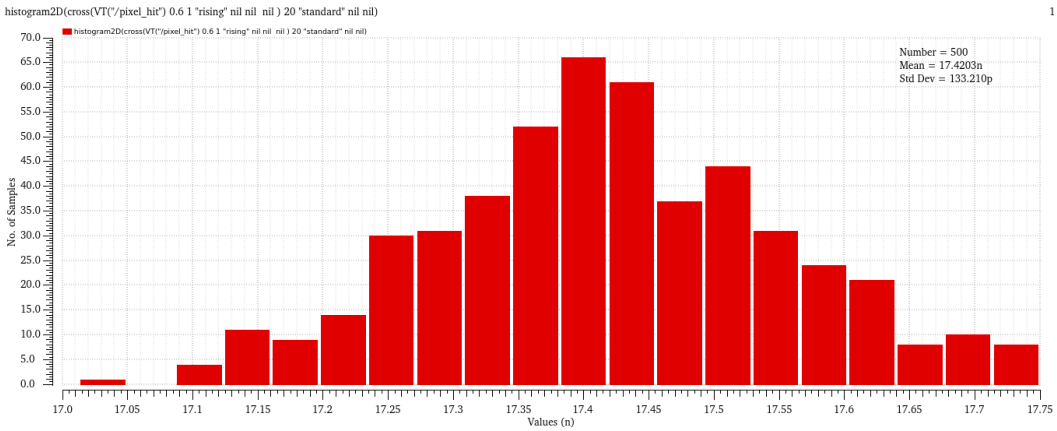

Figure 20: Hit leading edge timing distribution for an input charge of 6000 electrons. Input signal is applied at 10 ns.

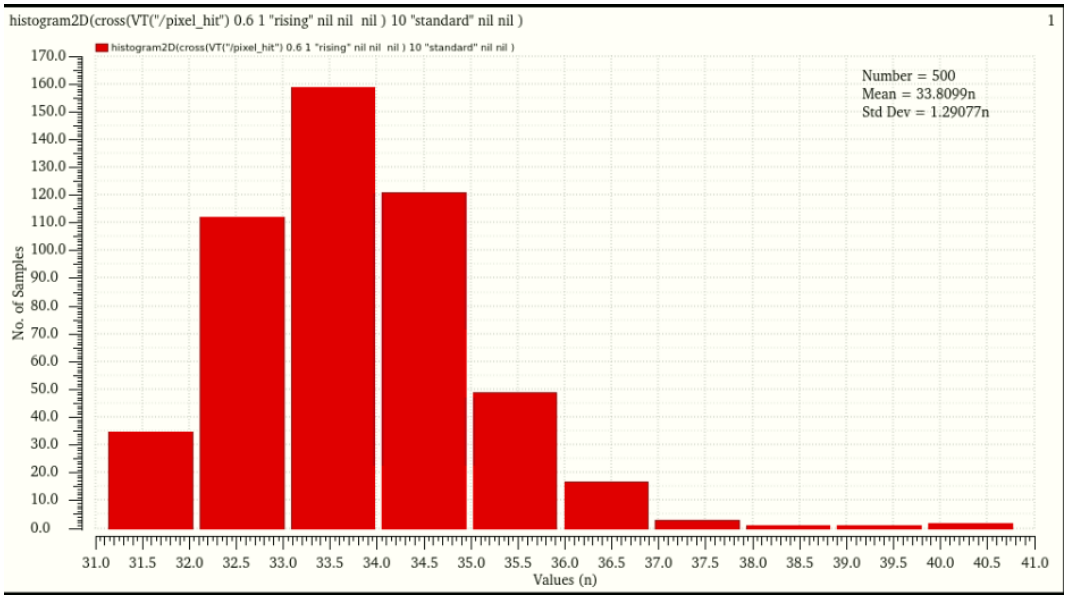

Figure 21: Hit leading edge timing distribution for an input charge of 1200 electrons. Input signal is applied at 10 ns.

3.1.4 Front-end behavior at different Krummenacher currents

A number of simulations were carried on the CMS FE in order to evaluate its behavior at different Krummenacher currents (i.e. different ToTs for the same input charge). Fig. 22

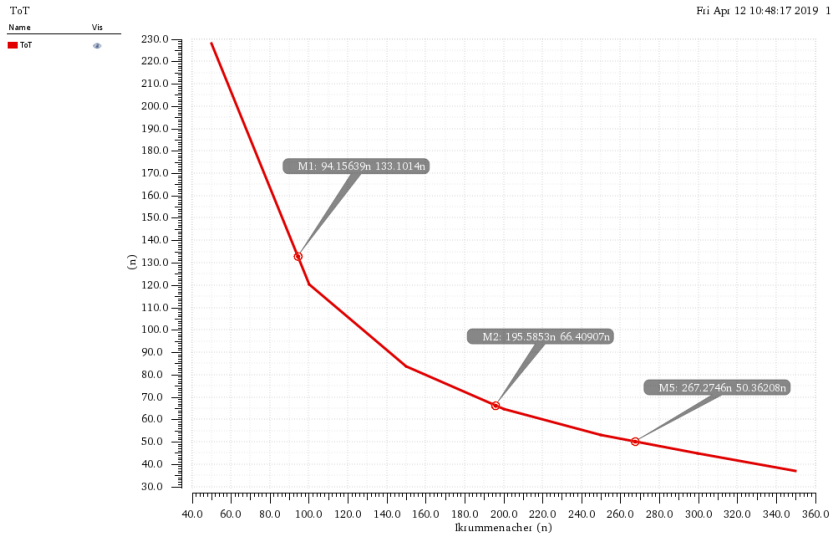

Figure 22: ToT as a function of the krummenacher current for an input charge of 6ke. The pixel Krummenacher current can be obtained by dividing by 10 the values reported on the x-axis.

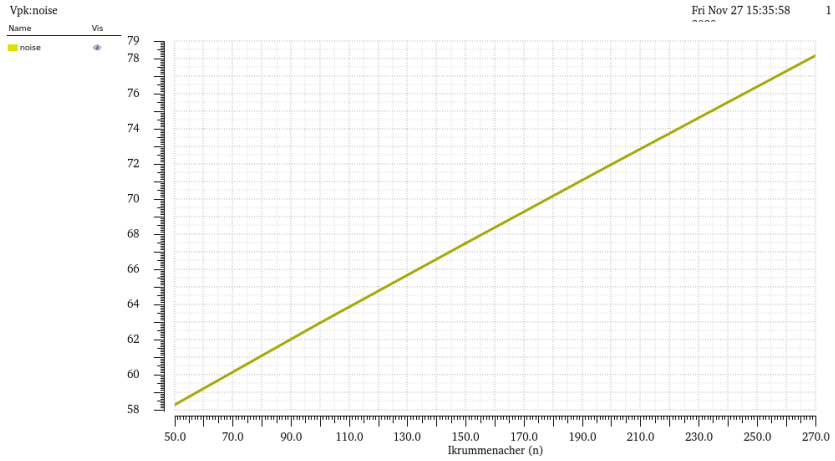

Figure 23: ENC as a function of the Krummenacher current. The pixel Krummenacher current can be obtained by dividing by 10 the values reported on the x-axis.

show the Time-over-Threshold (in ns) for an input charge of 6ke as a function of the Krummenacher current (the pixel value of such a current is obtained by dividing by 10 the values

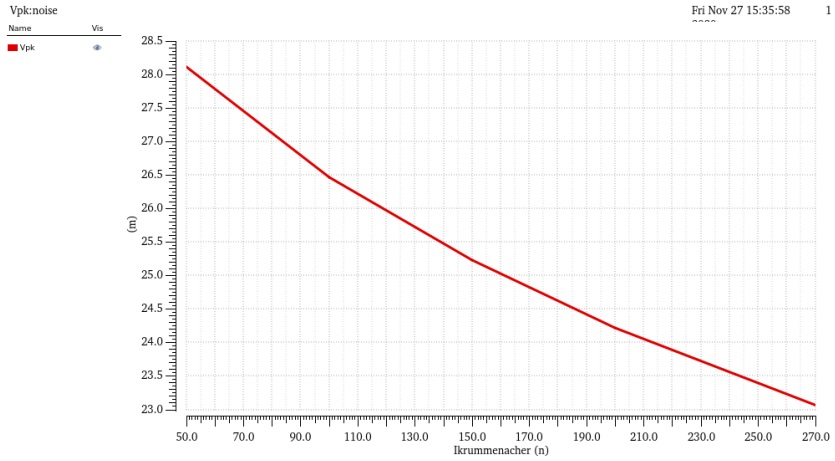

Figure 24: Charge sensitivity (mV/ke) as a function of Krummenacher current. The pixel Krummenacher current can be obtained by dividing by 10 the values reported on the x-axis.

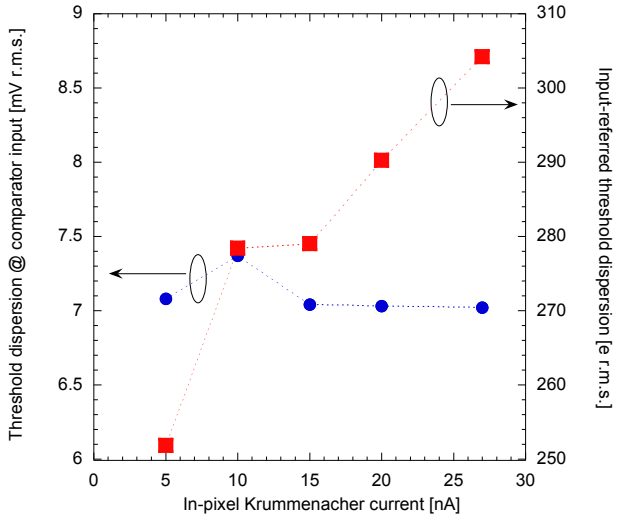

Figure 25: Threshold dispersion (evaluated at comparator input, in mV r.m.s. and at the front-end input, in e r.m.s., as a function of the Krummenacher current.

reported on the x-axis). Notice that simulations reported in the previous sections has been carried out by setting a ToT close to 133 ns for an input charge of 6ke. Such a condition is obtained by setting a Krummenacher current in the pixel close to 9 nA. The ToT can

be halved by setting a Krummenacher current close to 20 nA.
Fig. 23 shows the Equivalen Noise Charge (ENC, in electrons r.m.s.) as a function of the Krummenacher current. In the considered range of current a linear increase in the ENC is detected.
Fig. 24 shows the charge sensitivity (in mv/ke) as a function of the Krummenacher current. In the nominal ToT setting the charge sensitivity is close to 26 mV/ke, while the sensitivity evaluated at a Krummenacher current of 27 nA is reduced by 10%.
Threshold dispersion, evaluated at the comparator input, turns out to be almost independent of the Krummenacher current. Nonetheless, the FE input-referred threshold dispersion slightly increase with Krummenacher current due to the decrease in charge sensitivity, as shown in Fig. 25.

3.1.5 Voltage drop, temperature and leakage current effects

Voltage drop on power supplies, temperature gradients on the chip and detector leakage current effects on the main analog parameters have been investigated in the Typ OP corner. Fig. 26 shows the time-walk as a function of the input charge for voltage drops of 0 (red curve), 10 (yellow curve) and 20 mV (green curve) on both analog and digital power supplies (remember: the comparator output buffer lies in the digital domain). It is possible to notice a slight increase (around 7%) of time-walk for input signals close to the threshold for the maximum voltage drop. Such an increase has to be mainly ascribed to the reduced current in the preamplifier input branch attained at the maximum voltage drop (top pixels in the matrix). This result could be considered as a worst case for two reasons: first, the

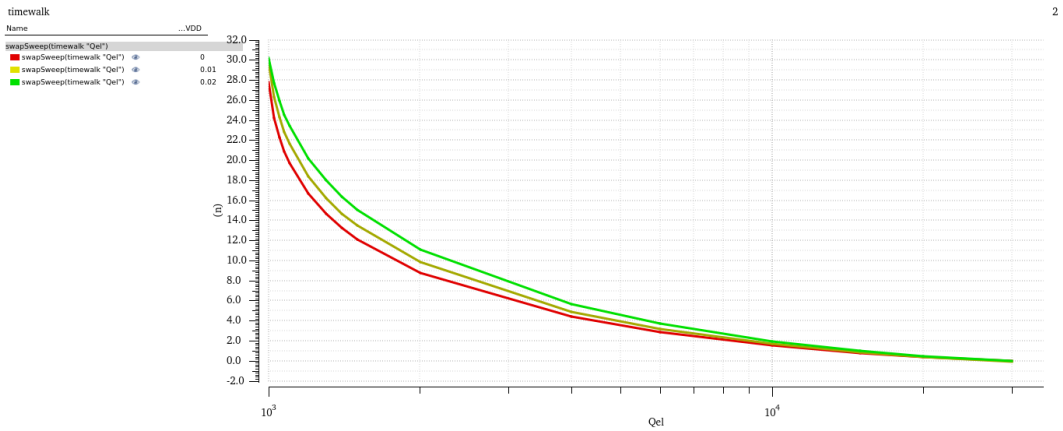

Figure 26: Time-walk as a function of the input charge for voltage drops of 0 (red curve), 10 (yellow curve) and 20 mV (green curve).

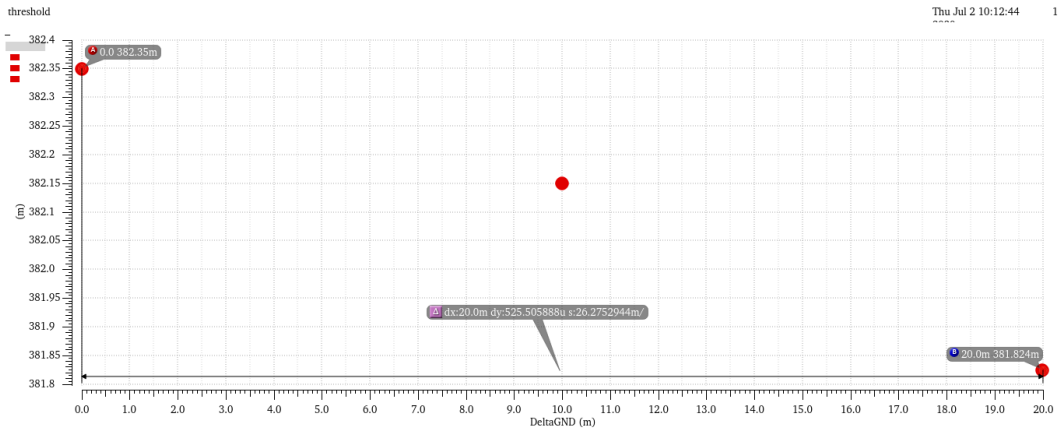

Figure 27: Effective comparator threshold as a function of voltage drop.

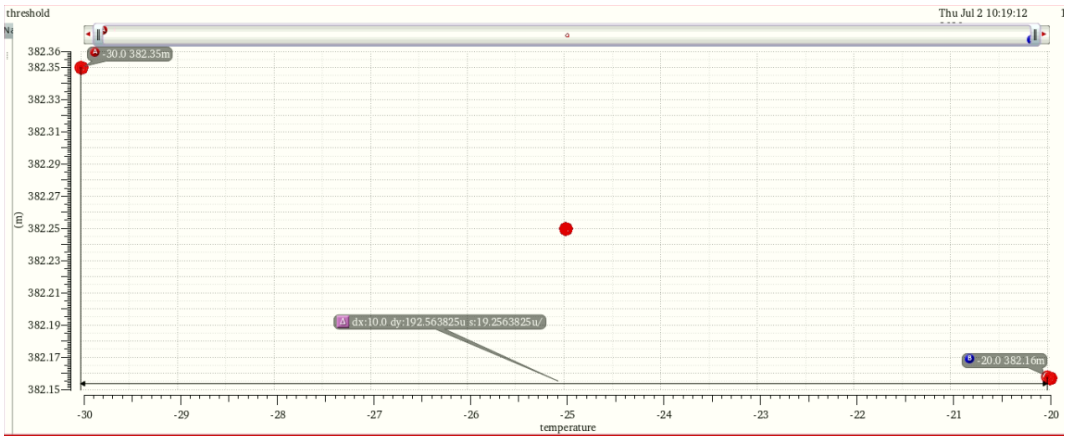

Figure 28: Effective comparator threshold as a function of temperature.

maximum simulated voltage drop of 20 mV is probably too pessimistic. Second, the pixel with no voltage drop (bottom pixels in the matrix) has been tuned to a total analog current of 5 μA: in actual operations, the total analog current of the matrix will be tuned in such a way to get a mean per-pixel value of 5 μA, resulting in higher currents for bottom pixels of the matrix and improved time-walk performance of the front-end.

Figs. 27 and 28 show the effective threshold, at comparator input, as a function of the voltage drop and chip temperature, respectively. The threshold variation at 20 mV voltage drop is around 525 μV. Such a variation is significantly smaller than the un-tuned threshold dispersion, around 7.4 mV, and can be easily compensated for by means of threshold tuning.

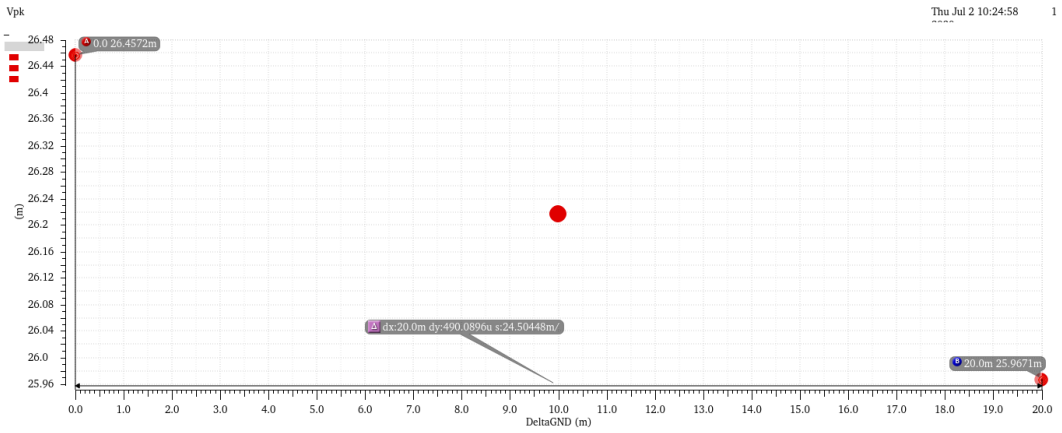

Figure 29: Preamplifier charge sensitivity as a function of voltage drop.

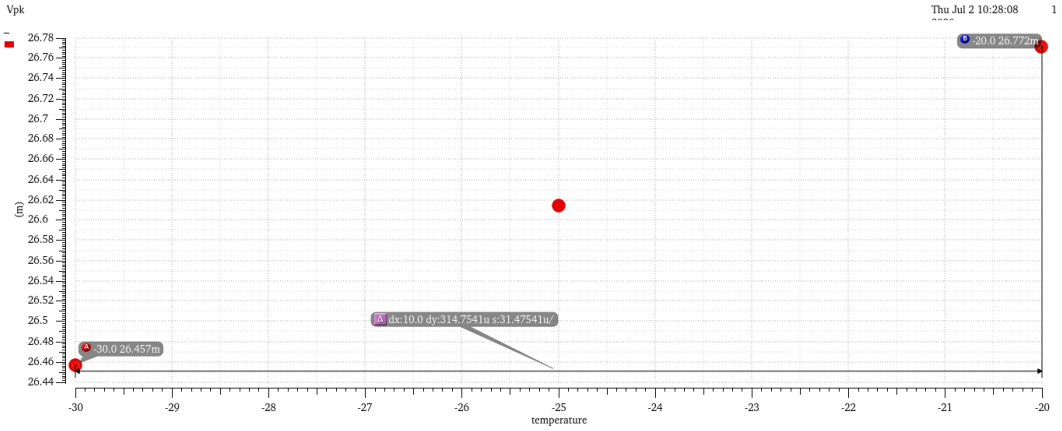

Figure 30: Preamplifier charge sensitivity as a function of temperature.

Same considerations hold for threshold variations with temperature: as shown in Fig. 28 the threshold shift for a temperature gradient of 10°C (from -30°C to -20°C) is of the order of 200 μV, again, negligible with respect to the un-tuned threshold dispersion.

The effects of voltage drop and temperature have been evaluated also on the CSA charge sensitivity. Fig. 29 shows the charge sensitivity G_q as a function of the voltage drop. The sensitivity decreases almost linearly with voltage drop, with a maximum variation close to 500 μV/ke$^-$ at 20 mV voltage drop. Such a variation has to be compared to the G_q obtained without voltage drop, of the order of 26 mV/ke$^-$.

Fig. 30 shows the charge sensitivity G_q as a function of the temperature, for temperatures

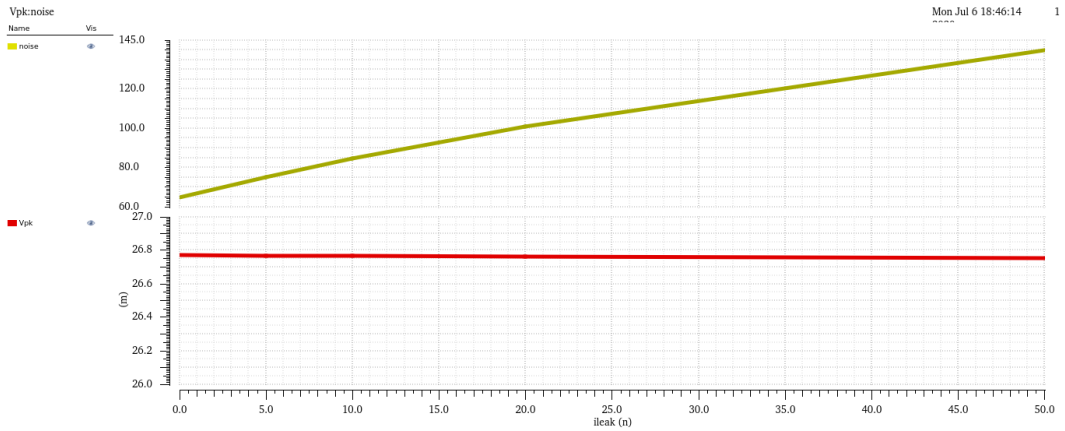

Figure 31: ENC (top) and preamplifier charge sensitivity (bottom) as a function of the detector leakage current.

ranging from -30°C to -20°C. In this case, an almost linear increase of charge sensitivity with temperature has been detected, with a maximum shift of the order of 315 μV/ke$^-$ to be compared, again, with G_q simulated without voltage drop.
As far as the detector leakage current is concerned, simulations on noise, charge sensitivity, ToT and threshold dispersion have been carried out. Fig. 31 shows the equivalent noise charge (top plot) and the preamplifier charge sensitivity (bottom plot) as a function of the detector leakage current. Notice that the detector leakage in this simulation spans from 0 to 50 nA, a value that is considerably larger than the expected radiation-induced detector leakage current. As expected, the noise increases with the detector leakage current, with an increase of the order of 30% for a current of 10 nA. No significant variations in the charge sensitivity were detected.

Fig. 32 shows the Time-over-Threshold as a function of the detector leakage current for an input charge of 6000 electrons. As for the previously discussed simulations, the results shown in the figure have been obtained without retuning of the bias currents. The ToT variation for a detector leakage current of 10 nA is fairly small, of the order of 500 ps, while it significantly increases for larger detector currents, with a ToT shift close to 5 ns for the maximum simulated leakage.
Fig. 33 shows the un-tuned threshold dispersion for the RD53A Linear front end (red) and for the CMS FE (blue). A clear trend, common to the two versions of the front-end, did not emerged from the simulations: the threshold dispersion is not significantly affected by leakage current for the RD53A version of the front-end, where as a slightly lower dispersion is achieved for the CMS FE at higher detector leakage currents.

Fig. 34 shows the preamplifier input voltage as a function of the detector leakage current in the TT_OP corner. Negative currents actually flow towards the preamplifier input; this

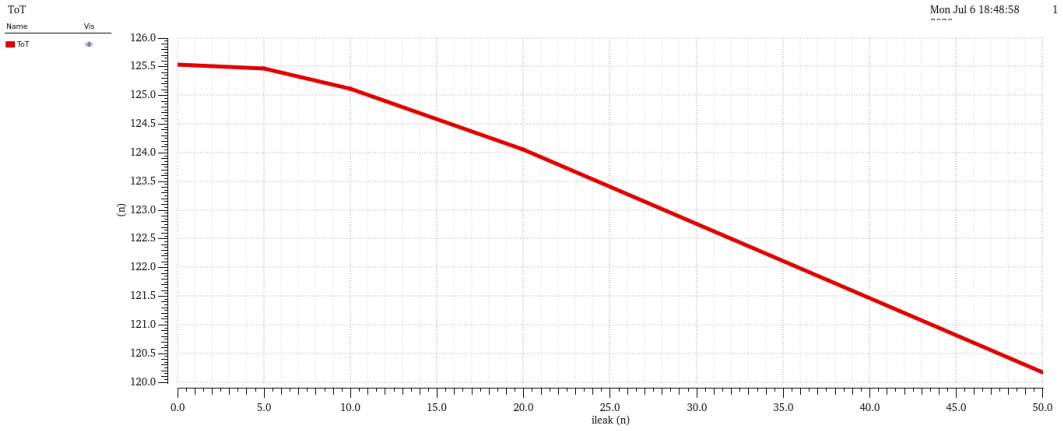

Figure 32: ToT as a function of the detector leakage current, for 6000 electrons input charge.

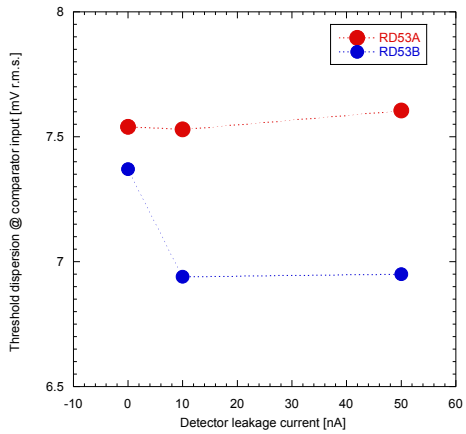

Figure 33: Un-tuned threshold dispersion as a function of the detector leakage for the RD53A Linear front-end (red) and for the CMS FE (blue).

could be generated by a forward-biased sensor, whereas positive leakage currents flow in the opposite direction, as in the case of radiation-induced sensor leakage. A negative current around 22 nA results in a preamplifier input voltage of 1.2 V. Notice that positive values of the current result in a stable preamplifier input voltage close to 425 mV, depending on the preamplifier input bias current. The value of the detector current at which the preamplifier input voltage gets to 1.2 V has been simulated by means of Monte-Carlo simulations, as shown in Fig. 35. The mean value of such a current is close to -22 nA with a very low

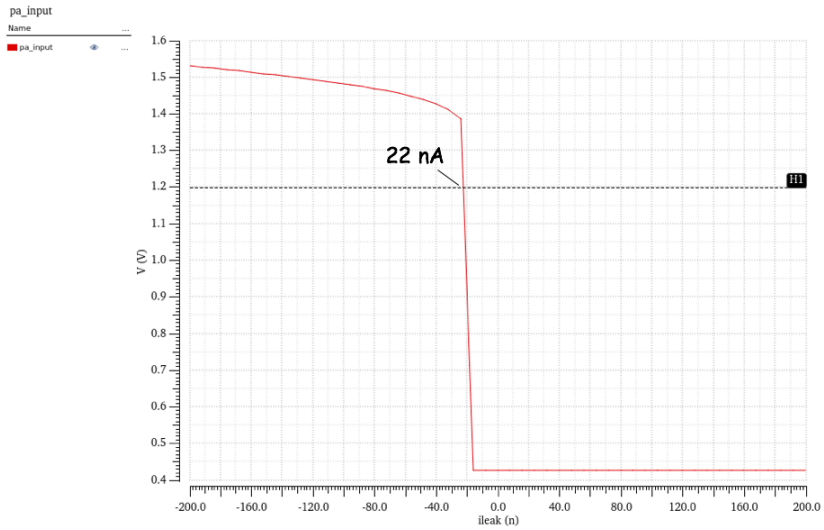

Figure 34: Preamplifier input voltage as a function of the detector leakage current. Negative values represent currents flowing towards the preamplifier input (forward-biased sensor).

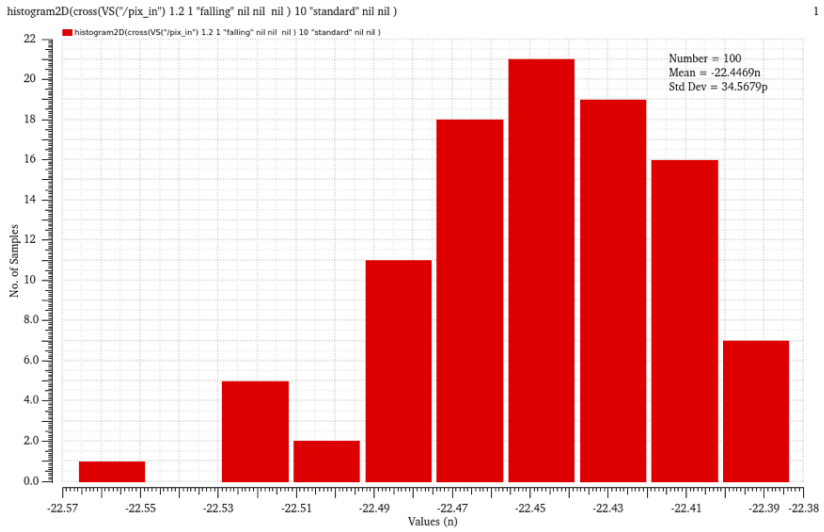

Figure 35: Detector current at which the preamplifier input voltage gets to 1.2 V (100 runs Monte-Carlo simulation).

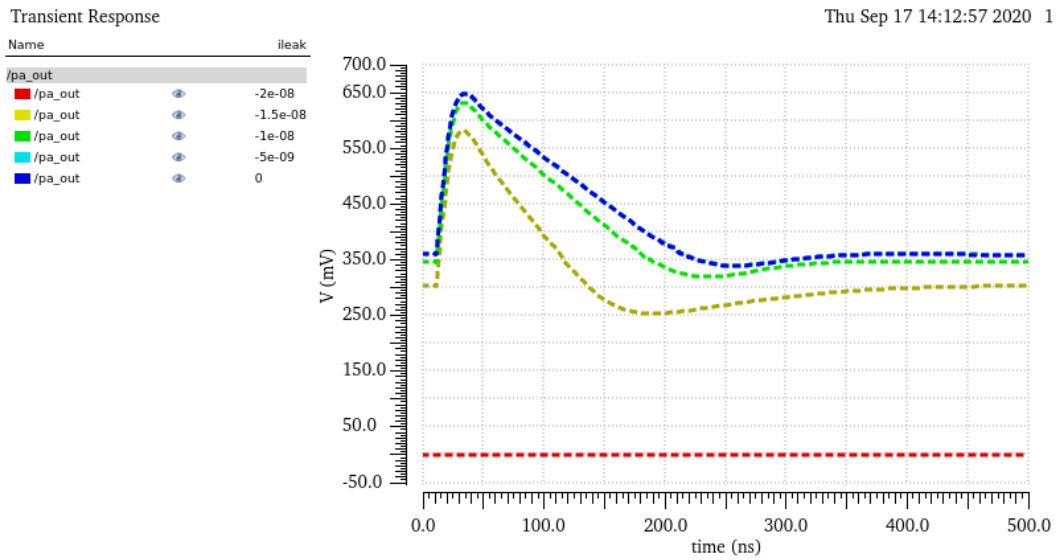

Figure 36: Preamplifier output in response to a 10ke signal for detector current ranging from 0 to -20 nA.

dispersion.
Fig. 36 shows the preamplifier output response to a 10ke signal for detector current ranging from 0 to -20 nA. Notice that for the maximum simulated current of -20 nA (red curve) the preamplifier is basically stuck to 0 V (no hits can thus be generated by the comparator). This feature may be exploited in order to check open bump-bonds, by forcing the detector in forward-bias and by checking the FE standard operation.

3.1.6 Cross-talk

Cross-talk simulations have been carried out for the TT_OP corner for two different sensor geometries, 25x100 and 50x50, involving different inter-pixel capacitances. The block diagram of the simulated circuit is shown in Fig. 37, with Ct, Cb, Cr and Cl being the inter-pixel capacitances whose values are provided in the same figure. Cross-talk has been evaluated as the ratio between the charge threshold of the central pixel C, set to 1000 electrons, and the charge needed to fire the comparator of T, R, B, and L pixels while injecting pixel C. Cross-talk results are gathered in Tab. 5, which shows a worst case for

the 25x100 sensor due to the large inter-pixel capacitance between pixel C and T (37 fF).

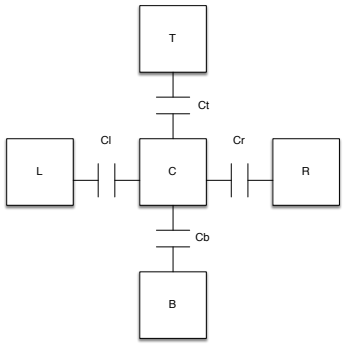

Sensor	Ct [fF]	Cr [fF]	Cb [fF]	Cl [fF]
25x100	37	3	12	3
50x50	10	10	10	10

Figure 37: Block diagram of the circuit for x-talk simulations. Ct, Cb, Cr and Cl are the inter-pixel capacitances, whose values are shown in the table on the right-hand side.

3.1.7 Response to large signals

Fig. 38 shows the preamplifier (top) and comparator (bottom) output response to an input signal of 100000 electrons. Charge injection takes place at t=10 ns, and the full recovery of the baseline, around 360 mV for the TT_OP corner, takes places at t=8 μs. The ToT for that corner is close to 2 μs.

3.2 500 Mrad results at 0°C

3.2.1 Power supply current, noise and charge sensitivity

Fig. 39 shows the total analog current drawn by the single pixel. As mentioned, the FE has been tuned to 5 μA in the 500 Mrad TT corner. The plot reveals a maximum current in the FF 1.32V corner (5.4 μA) and a minimum in the SS 1.08V corner (4.7 μA).
Fig. 40 shows the ENC as a function of the detector capacitor C_D for the different corners, for C_D ranging from 0 to 200 fF. For the sake of comparison, the plot also shows data for the Typ OP corner (red curve). With respect to the Typ OP corner, an ENC increase around 16% has been detected for the 500 Mrad corners at 0°C.

Table 5: Cross-talk simulation results

Sensor geometry	T	R	B	L
25x100	20.0%	2.6%	8.3%	2.6%
50x50	6.9%	6.9%	6.9%	6.9%

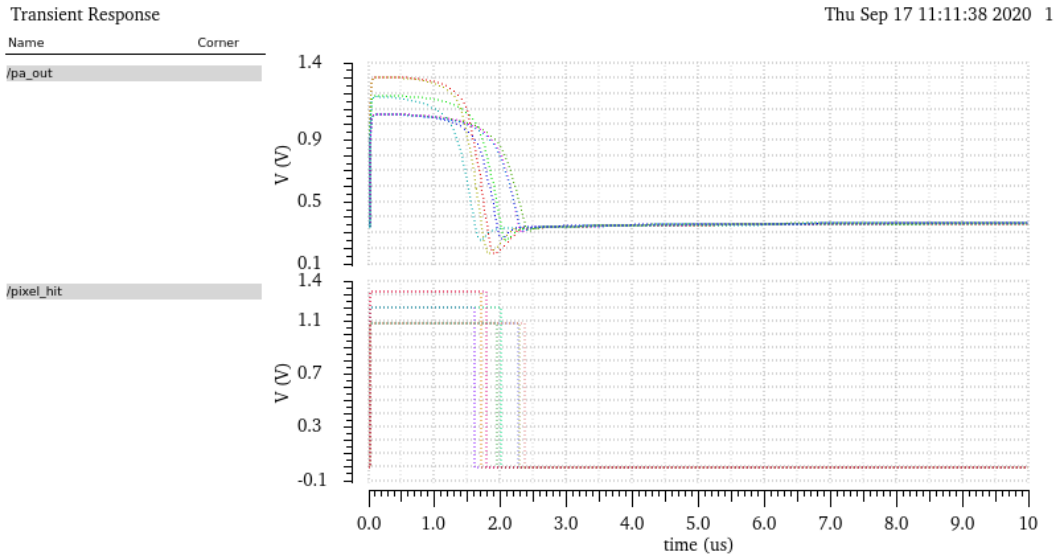

Figure 38: Preamplifier (top) and comparator (bottom) output response to an input charge of 100000 electrons.

Fig. 41 shows the CSA charge sensitivity, G_q (in mV/ke$^-$), in the different corners. A G_q around 27.5 mV/ke$^-$ has been obtained in the 500 Mrad TT corner, slightly higher than the G_q obtained in the Typ OP corner (26.5 mV/ke$^-$). As for the pre-rad scenario, main contributions to the charge sensitivity fluctuations are the variations of the CSA feedback

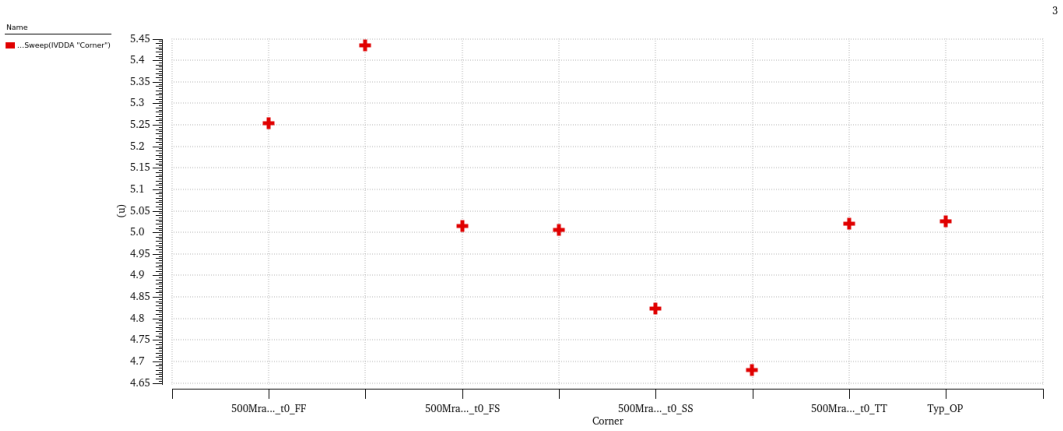

Figure 39: Analog power supply current in the different corners.

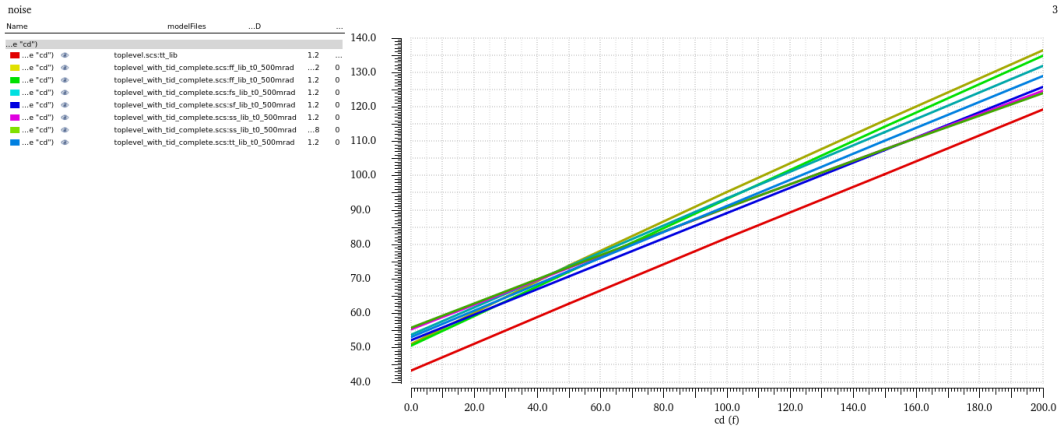

Figure 40: Equivalent noise charge as a function of the detector capacitance.

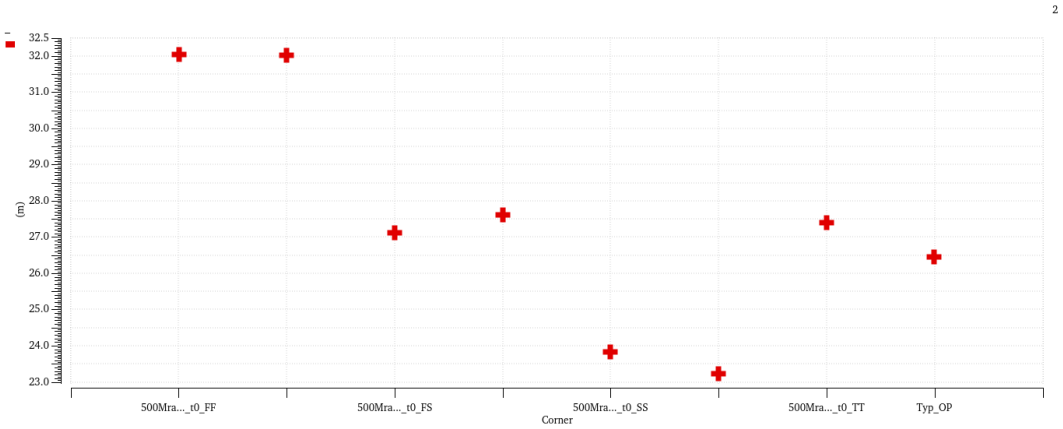

Figure 41: Preamp charge sensitivity G_q for the simulated corners.

capacitance and of the Krummenacher feedback current (not tuned in the different corners).

3.2.2 Threshold dispersion and TDAC range

Fig. 42 shows the threshold distribution for the 500 Mrad TT corner. Threshold is evaluated at the comparator input, in mV, by means of DC sweeps of the global threshold. The distribution features a standard deviation, σ_{Vth}, of 7.7 mV, which can be converted into electrons, as explained in the previous section, by dividing by the CSA charge sensitivity

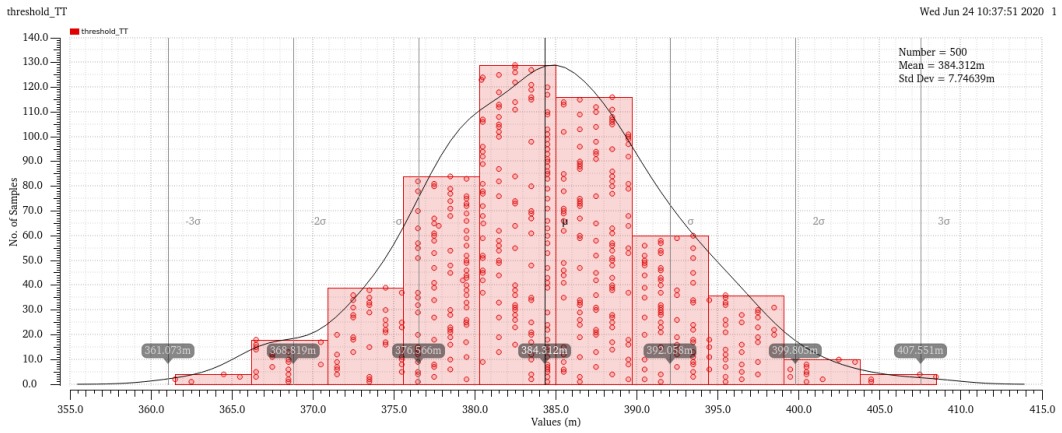

Figure 42: Un-tuned threshold distribution for the 500 Mrad TT corner. Threshold is evaluated at the comparator input (in mV).

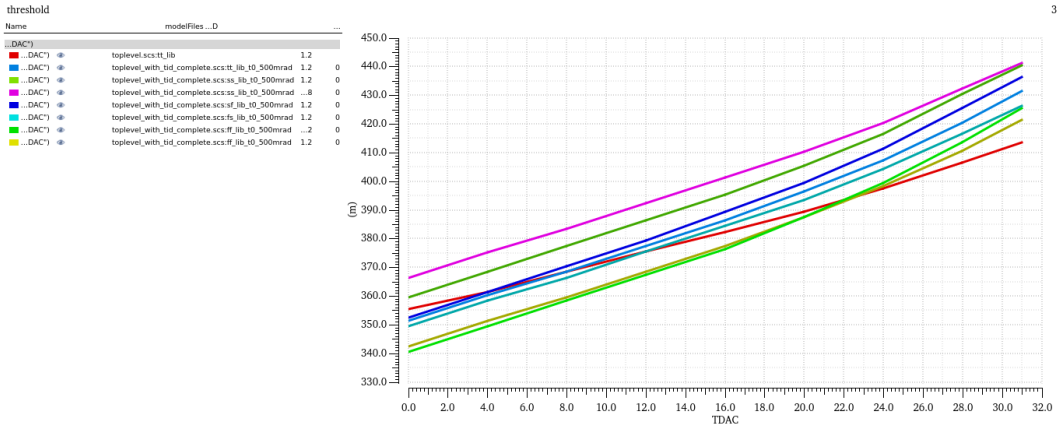

Figure 43: Comparator effective threshold (in mV) as a function of the TDAC code, for LDAC_LIN=140.

G_q, resulting in an un-tuned threshold dispersion, σ_{Qth}, around 300 electrons. From circuit simulations a TDAC dynamic range around 46 mV ($6 \times \sigma_{Vth}$) is thus required in order to compensate for the threshold dispersion.
Fig. 43 shows the effective threshold (evaluated, in mV, at the comparator input) as a function of the TDAC code, for LDAC_LIN set to 140. For the different corners, a TDAC dynamic range (i.e. the difference between threshold at TDAC=31 and the one obtained at TDAC=0) around 70 mV has been obtained. For the sake of comparison, data for the

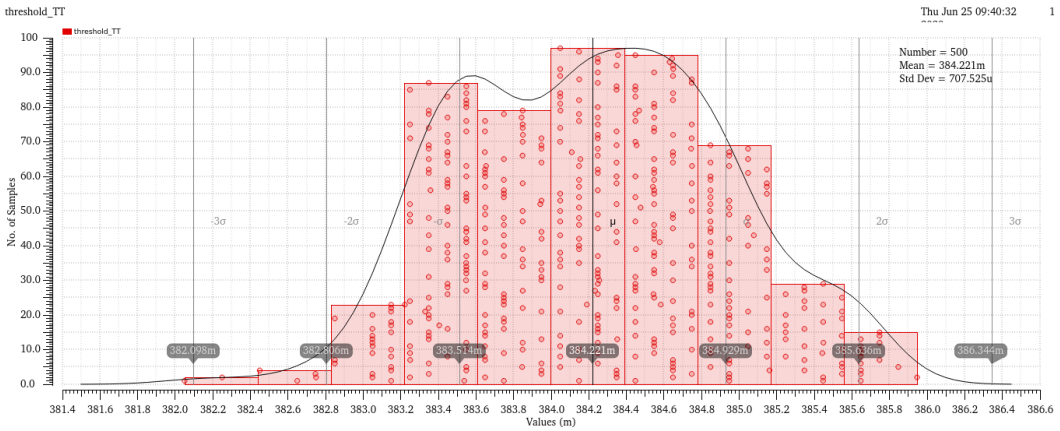

Figure 44: Tuned threshold distribution for the 500 Mrad TT corner. Threshold is evaluated at the comparator input (in mV).

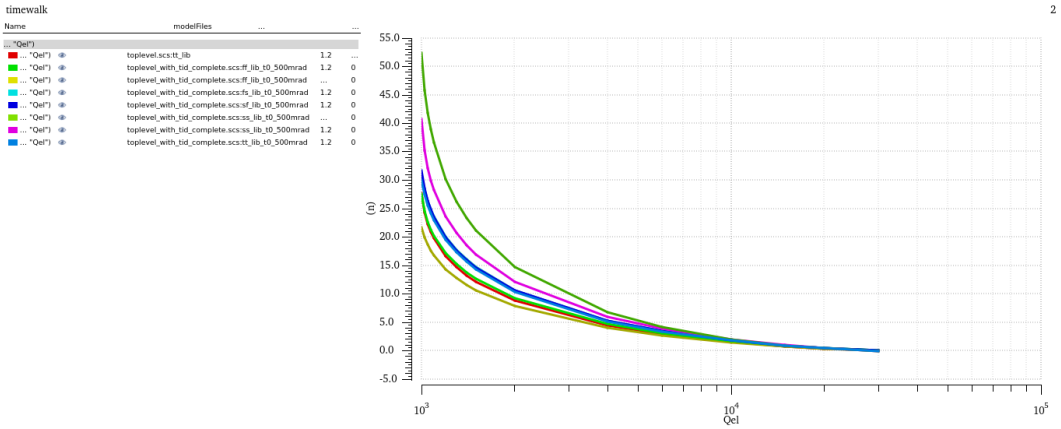

Figure 45: Time-walk as a function of the input charge (log-scale x-axes).

Typ OP corner are shown (red curve): notice the different slope of the characteristics for the 500 Mrad corners, which can be explained by a reduced current in the comparator input stage, resulting in a smaller transconductance of the stage and, in turn, in a larger TDAC dynamic range. Again, it is possible to translate the dynamic range in electrons at the FE input by dividing by G_q, resulting in a range close to 2500 electrons.

As mentioned in the previous section, an Ocean script has been developed in order to simulate the tuned threshold dispersion of the CMS FE. Fig. 44 shows the threshold distribution after trimming for the 500 Mrad TT corner. Notice that the standard deviation

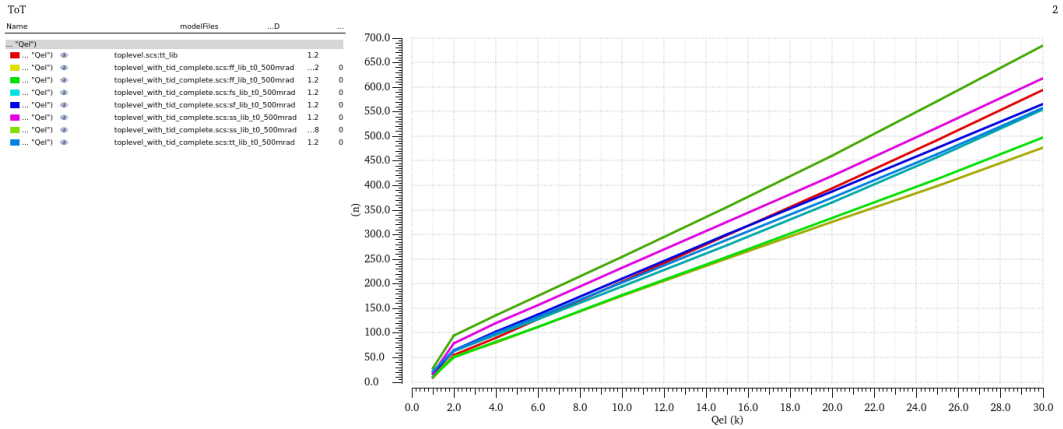

Figure 46: Time-over-Threshold as a function of the input charge (lin-scale x-axes).

of the distribution, around 707 μV, is reduced by a factor close to 10 with respect to the pre-tuning value.

3.2.3 Timewalk and Time-over-Threshold

Fig. 45 shows the time-walk as a function of the input charge, for signals ranging from 1000 to 30000 electrons (log-scale on x-axes). Pre-rad simulation data (red curve) has been added to the plot for the sake of comparison. With respect to the pre-rad data, a slightly larger time-walk has been obtained in the 500 Mrad TT corner (light blue curve). On the other hand, a non-negligible increase in time-walk is detected for some of the 500 Mrad corners, in particular the SS 1.08V one.
Fig. 46 shows the Time-over-Threshold (ToT) for input charge signals ranging from 1000 to 30000 electrons (lin-scale on x-axes). As for the pre-rad data, a good linearity for signals larger than 2000 electrons is achieved.

Fig. 47 shows the ToT distribution for an input charge of 6000 electrons, obtained after threshold trimming by means of 500 runs of a Monte-Carlo simulation. The mean ToT value, with KRUM_CURR_LIN register set to 70, is close to 130 ns with a standard deviation of 11.2 ns. A slightly larger ToT dispersion is obtained with the un-tuned matrix (16.0 ns). A very small time dispersion of the hit leading edge signal has been obtained, as shown in Fig. 48, which shows the time distribution of the hit signal for an input charge of 6000 electrons (notice the small standard deviation).

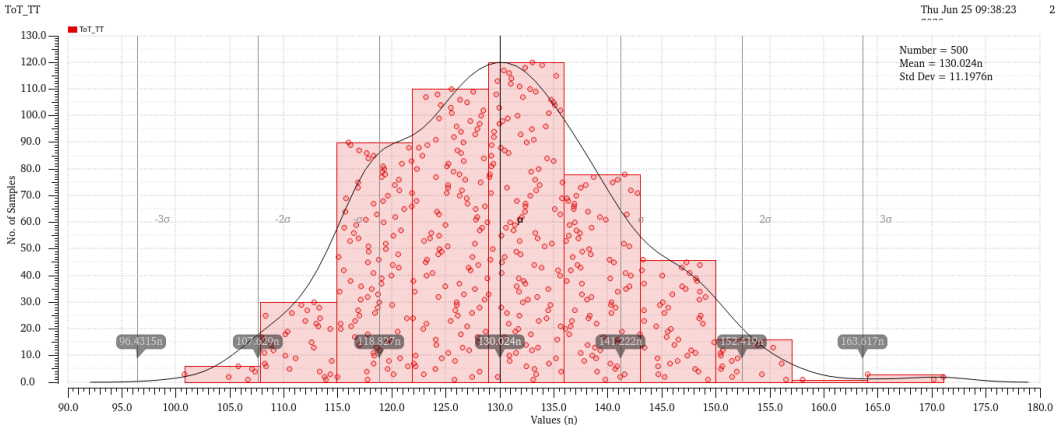

Figure 47: ToT distribution for an input charge of 6000 electrons. Data obtained after threshold trimming.

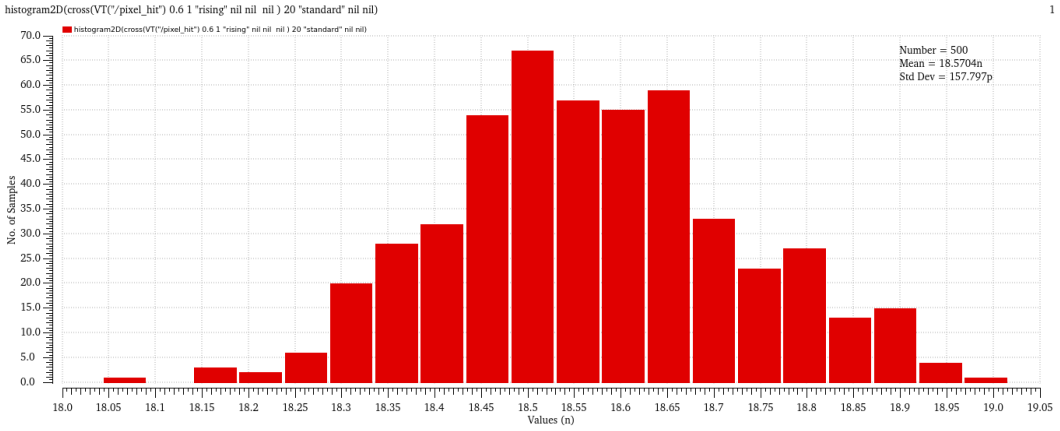

Figure 48: Hit leading edge timing distribution for an input charge of 6000 electrons. Input signal is applied at 10 ns.

3.2.4 Response to large signals

Fig. 49 shows the preamplifier (top) and comparator (bottom) output response to an input signal of 100000 electrons. Charge injection takes place at t=10 ns, and the full recovery of the baseline, around 360 mV for the TT_OP corner, takes places at t=9 μs. The ToT for that corner is close to 2 μs.

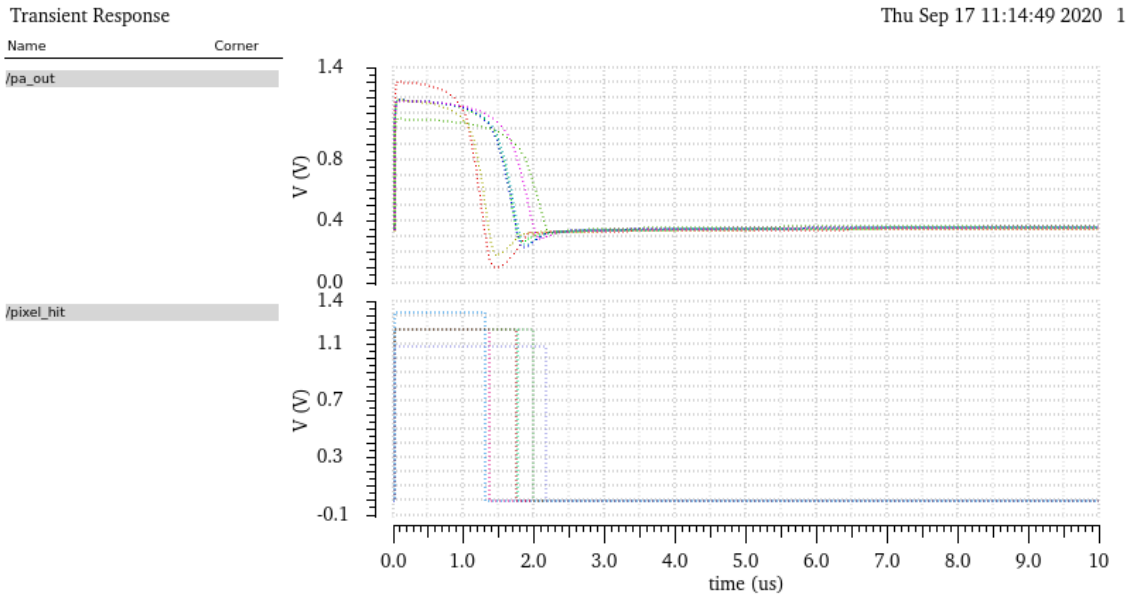

Figure 49: Preamplifier (top) and comparator (bottom) output response to an input charge of 100000 electrons.

3.3 500 Mrad results at -30°C

3.3.1 Power supply current, noise and charge sensitivity

Fig. 50 shows the total analog current drawn by the single pixel. As mentioned, the FE has been tuned to 5 μA in the 500 Mrad TT corner. The plot reveals a maximum current

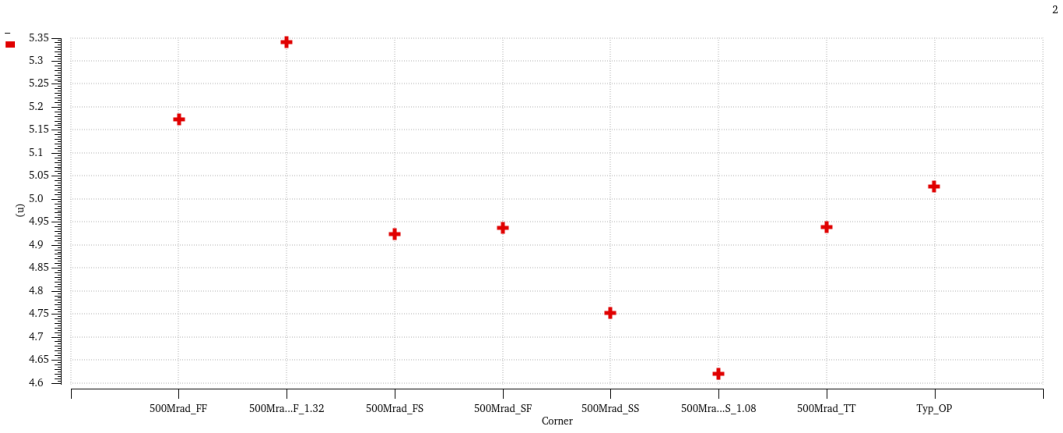

Figure 50: Analog power supply current in the different corners.

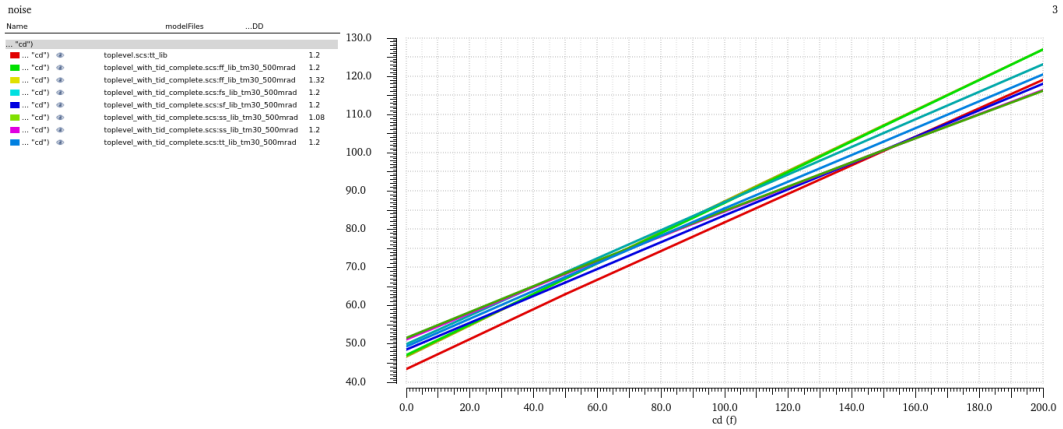

Figure 51: Equivalent noise charge as a function of the detector capacitance.

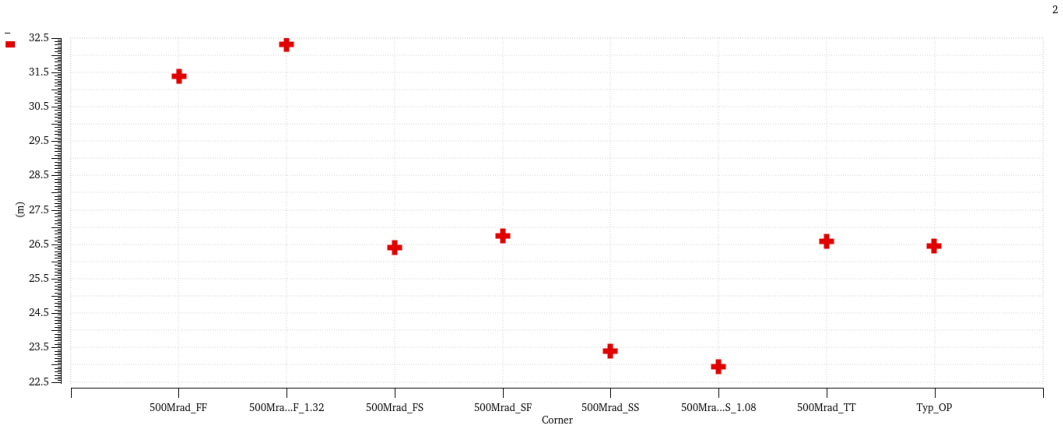

Figure 52: Preamp charge sensitivity G_q for the simulated corners.

in the FF 1.32V corner (5.3 μA) and a minimum in the SS 1.08V corner (4.6 μA).
Fig. 51 shows the ENC as a function of the detector capacitor C_D for the different corners, for C_D ranging from 0 to 200 fF. For the sake of comparison, the plot also shows data for the Typ OP corner (red curve). With respect to the Typ OP corner, an ENC increase around 8% has been detected for the 500 Mrad corners at -30°C.
Fig. 52 shows the CSA charge sensitivity, G_q (in mV/ke$^-$), in the different corners. A G_q around 26.5 mV/ke$^-$ has been obtained in the 500 Mrad TT corner, very close to the one obtained in the Typ OP corner. As for the pre-rad scenario, main contributions to the charge sensitivity fluctuations are the variations in the CSA feedback capacitance and of

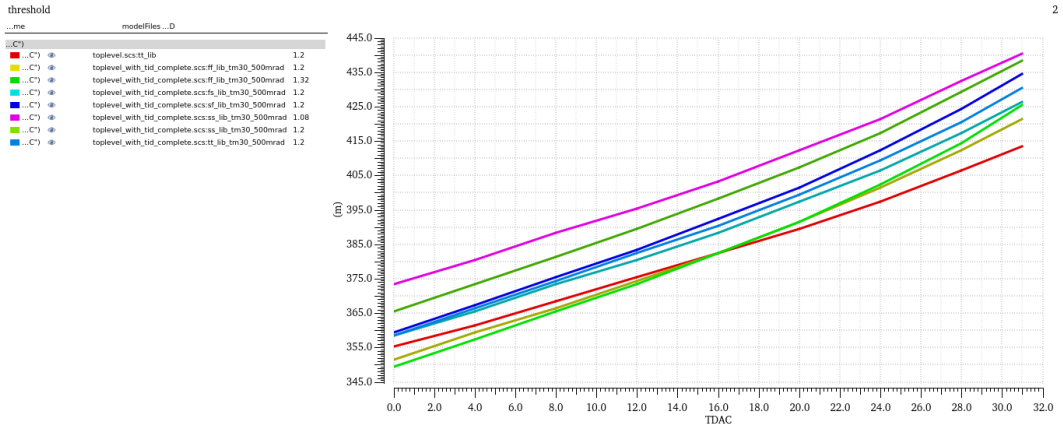

Figure 53: Comparator effective threshold (in mV) as a function of the TDAC code, for LDAC_LIN=140.

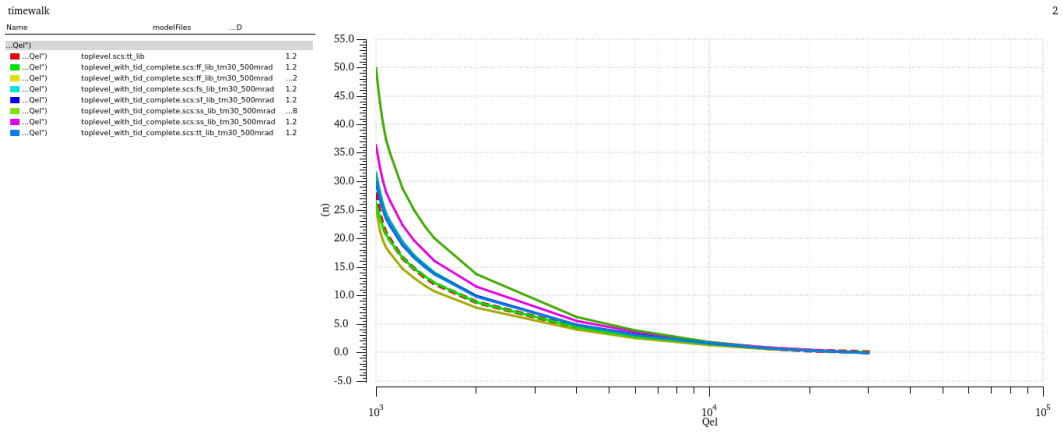

Figure 54: Time-walk as a function of the input charge (log-scale x-axes).

the Krummenacher feedback current (not tuned in the different corners).

3.3.2 TDAC range

Fig. 43 shows the effective threshold (evaluated, in mV, at the comparator input) as a function of the TDAC code, for LDAC_LIN set to 140. For the different corners, a TDAC dynamic range (i.e. the difference between threshold at TDAC=31 and the one obtained at TDAC=0) around 70 mV has been obtained. For the sake of comparison, data for the Typ OP corner are shown (red curve): notice the different slope of the characteristics for

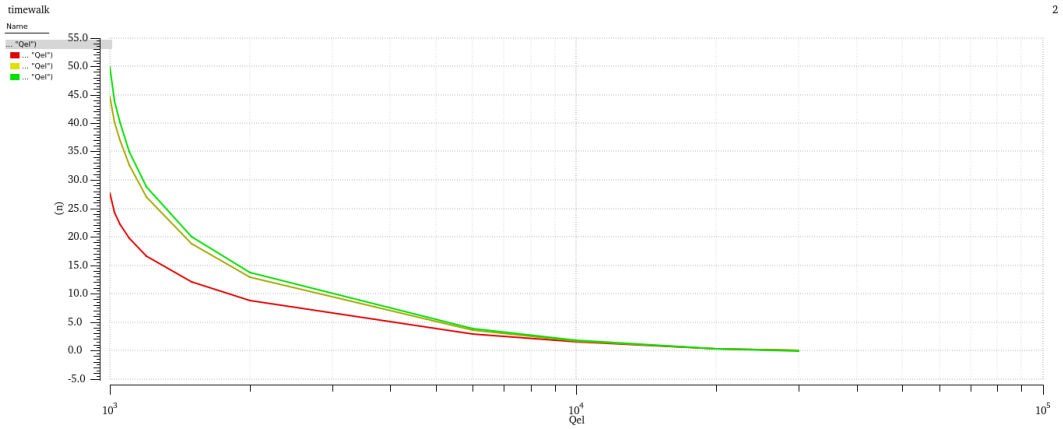

Figure 55: Time-walk as a function of the input charge for the TT corner, the SS 1.08V corner without bias re-tuning (green) and with bias retuning (yellow). For the sake of comparison, Typ OP data are reported (red).

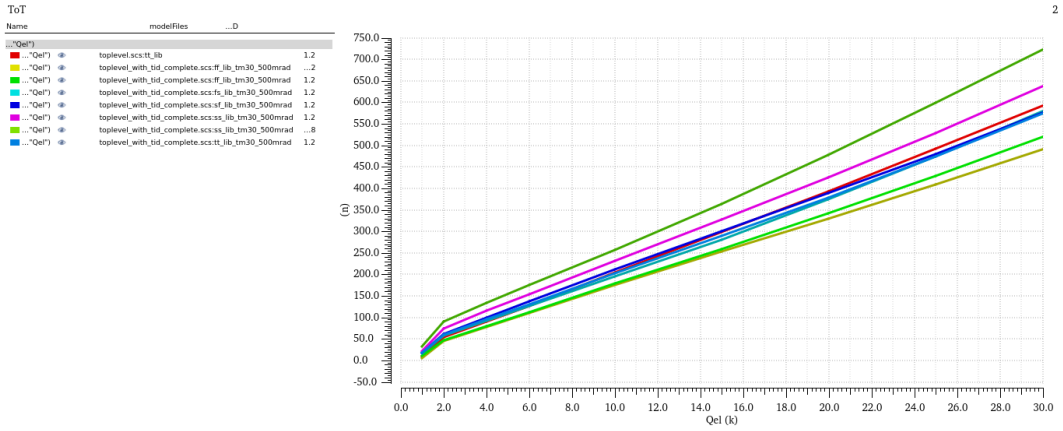

Figure 56: Time-over-Threshold as a function of the input charge (lin-scale x-axes).

the 500 Mrad corners, which can be explained by a reduced current in the comparator input stage, resulting in a smaller transconductance of the stage and, in turn, in a larger TDAC dynamic range. Again, it is possible to translate the dynamic range in electrons at the FE input by dividing by G_q, resulting in a range close to 2500 electrons.

3.3.3 Timewalk and Time-over-Threshold

Fig. 54 shows the time-walk as a function of the input charge, for signals ranging from 1000 to 30000 electrons (log-scale on x-axes). Pre-rad simulation data (dotted red curve) has been added to the plot for the sake of comparison. With respect to pre-rad data, a slightly larger time-walk has been obtained in the 500 Mrad TT corner (light blue curve). On the other hand, a non-negligible increase in time-walk is detected for some of the 500 Mrad corners, in particular the SS 1.08V one. As shown in Fig. 55 a partial recovery of time-walk can be achieved by retuning the total analog current in the analog front-end. In the figure, the green curve is relevant to the SS 1.08V corner without bias retuning, whereas the yellow one is the time-walk achieved by tweaking, in the same corner, the total current to 5 μA. Fig. 56 shows the Time-over-Threshold (ToT) for input charge signals ranging from 1000 to 30000 electrons (lin-scale on x-axes). As for the pre-rad data, a good linearity for signals larger than 2000 electrons is achieved.

3.3.4 Response to large signals

Fig. 57 shows the preamplifier (top) and comparator (bottom) output response to an input signal of 100000 electrons. Charge injection takes place at t=10 ns, and the full recovery of the baseline, around 360 mV for the TT_OP corner, takes places at t=8 μs. The ToT for that corner is close to 2 μs.

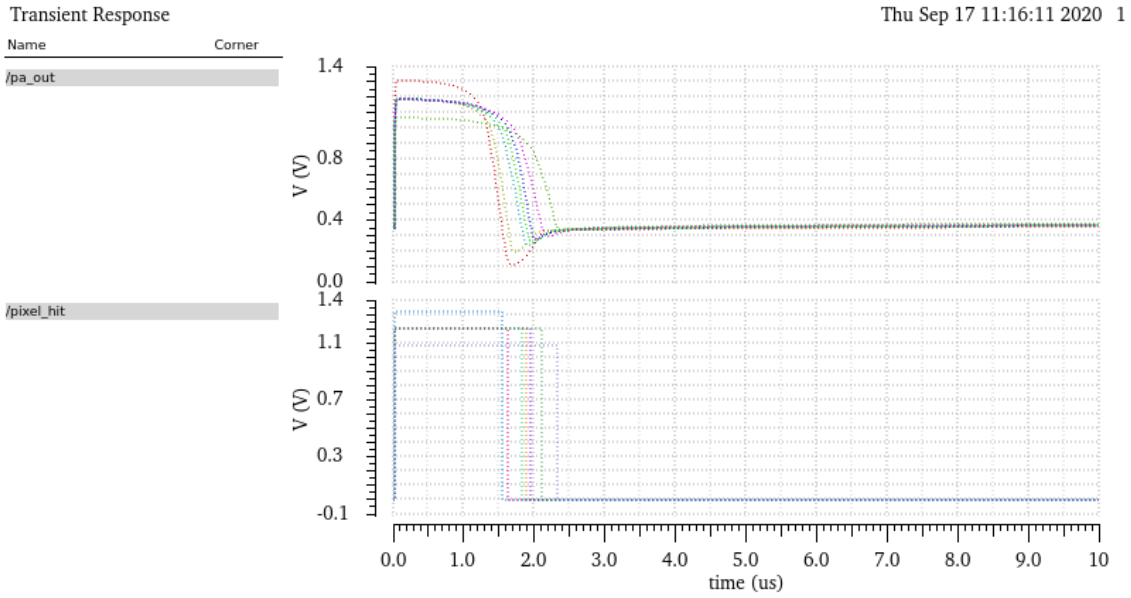

Figure 57: Preamplifier (top) and comparator (bottom) output response to an input charge of 100000 electrons.

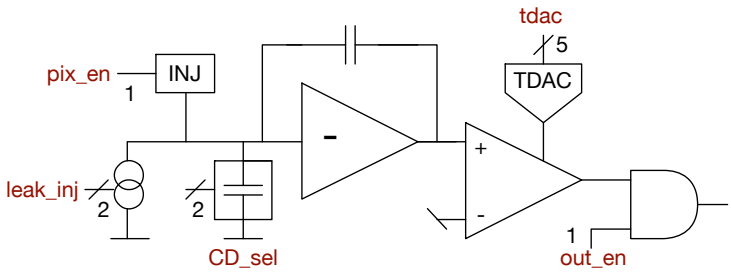

Figure 58: Block digram of the analog processor integrated in the prototype chip.

4 Prototype test results

A small prototype chip including the CMS front-end has been submitted and fully characterized. The submitted chip includes a matrix of 16×16 front-end channels with a pitch of 50 μm integrated in the so-called "analog islands" arrangement as in the RD53A chip. The matrix is divided in two equally sized regions featuring the Linear front-end (hereafter referred to as RD53A Linear front-end) and the CMS front-end (hereafter referred to as RD53B Linear front-end).
Fig. 58 shows the simplified schematic diagram of the analog front-end integrated in the prototype chip. The analog front-end includes the same injection circuit, featuring an injection capacitance of 8.5 fF, integrated in the RD53A front-ends. The front-end channel is equipped with two detector emulating capacitors of 50 fF and 100 fF which can be selectively shunted to the preamplifier input, thus enabling 4 different configurations (0, 50 fF, 100 fF and 150 fF). The preamplifier input can also be connected to a leakage injection circuit by means of a controllable CMOS switch. Such an injection circuit, based on simple NMOS and PMOS current mirrors shunting the gate of the preamplifier input transistor, emulates the DC detector leakage and can be used to generate both positive (NMOS mirror sinking current) and negative (PMOS mirror sourcing current) leakage currents.
The prototype has been characterized before and after exposure to TIDs up to 1 Grad of X-rays at a temperature close to -10°C. The dose rate during the irradiation was around 11 Mrad/h and the analog front-ends were biased with a per-pixel current consumption of 5 μA. Both analog and digital VDD was set to 1.2V. A detector capacitance of 50 fF was connected to the preamplifier inputs during the radiation campaign.
Two samples of the chip were irradiated in different bias conditions. In particular:

- Chip2: ToT set to 133ns for an input charge of 6ke (at room temperature). LDAC_LIN=130;
- Chip3B: ToT set to 70ns for an input charge of 6ke (at room temperature).

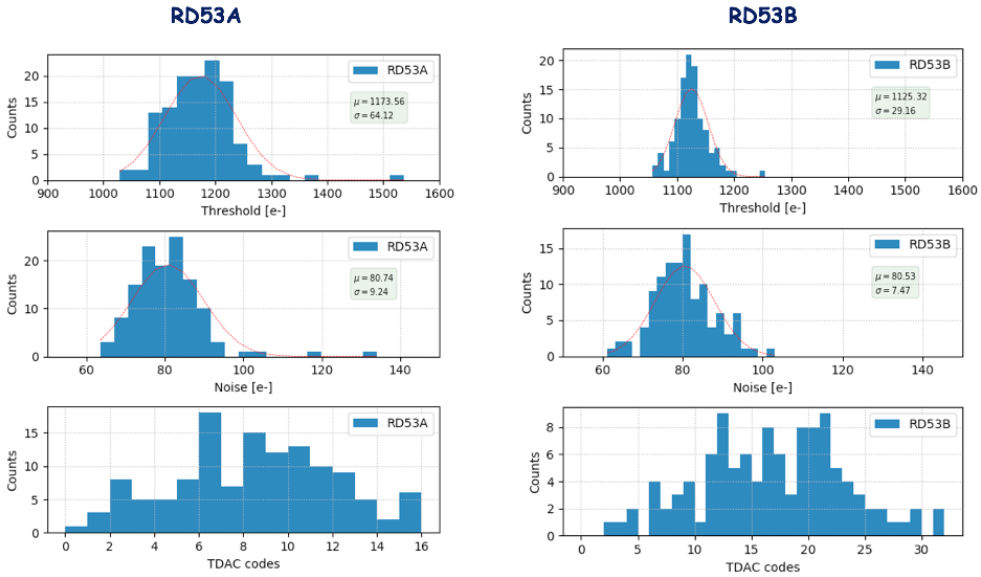

Figure 59: Threshold (first row), noise (second row) and TDAC codes (third row) distributions for the RD53A (left column) and RD53B (right column) front-ends.

LDAC_LIN=190.

4.1 Chip2: pre-rad results

Fig. 59 shows the tuned threshold (first row), noise (second row) and TDAC codes (third row) distributions for the RD53A front-end (left column) and the RD53B ones (right column). The target threshold for both RD53A and RD53B channels is close to 1100 electrons. Notice that the threshold dispersion for the RD53B version is around half the dispersion of the RD53A one. This is due to the additional trimming DAC bits integrated in the RD53B version, featuring a tuned-threshold dispersion close to 29 electrons, in good agreement with simulations. The equivalent noise charge for both the versions of the front-end is close to 80 electrons, with a slightly higher dispersion for the RD53A front-end.
Fig. 60 shows the time-walk as a function of the input charge for the two versions of the front-end. The plot on the right size is a zoom for input charges ranging from 1100 to 1600 electrons. Notice the significant smaller time-walk for the RD53B version, which confirms the improvement in time-walk already obtained in circuit simulations. In particular, a time-walk smaller than 25 ns has been measured for the RD53B FE for an input charge close to the threshold, whereas a time-walk of 35 ns has been detected for the RD53A version.
Fig. 61 shows the Time-over-Threshold as a function of the input charge for the RD53A

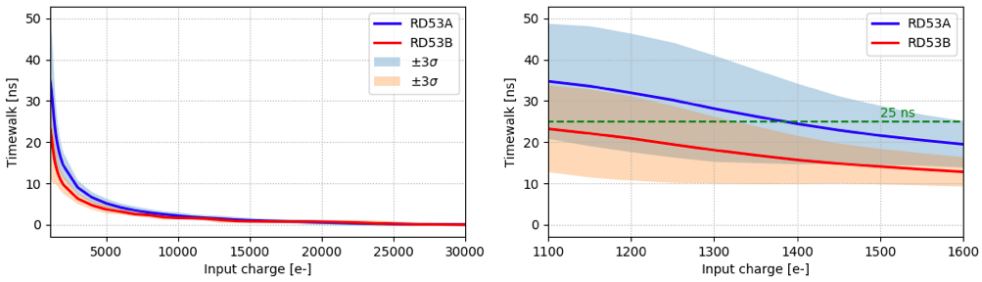

Figure 60: Time-walk as a function of the input charge for RD53A (blue curve) and RD53B (red curve) FEs. The plot on the right hand side is a zoom of the time-walk for input charges ranging from 1100 to 1600 electrons.

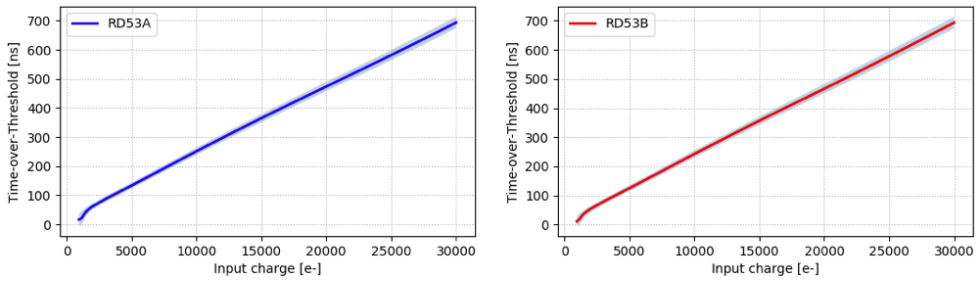

Figure 61: Time-over-Threshold as a function of the input charge for the RD53A (left plot) and the RD53B (right plot) front-ends.

(left plot) and the RD53B (right plot) front-ends. Both the front-ends have been biased in such a way to get a ToT close to 133 ns for an input charge of 6000 electrons. The tuning of the preamplifier discharge rate has been performed at room temperature and has not been tweaked after cooling down to -10°C. A pretty linear behavior of the ToT has been obtained for both the versions of the front-end for input charges larger than 2000 electrons.

4.2 Chip2: 1 Grad results

Fig. 62 shows the tuned threshold (first row), noise (second row) and TDAC codes (third row) distributions for the RD53A front-end (left column) and the RD53B ones (right column) after exposure to 1 Grad of X-rays. The mean threshold for RD53A and RD53B channels is close to 800 and 900 electrons, respectively. Notice that the threshold dispersion for the RD53B version is significantly smaller than the one measured for RD53A. The equivalent noise charge, slightly larger with respect to pre-rad values, is close to 90 electrons

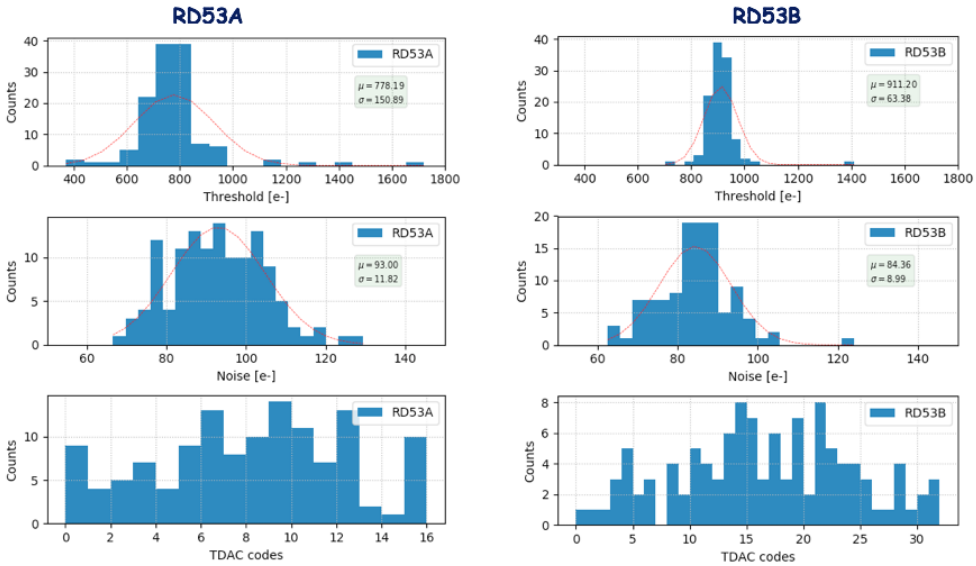

Figure 62: Threshold (first row), noise (second row) and TDAC codes (third row) distributions for the RD53A (left column) and RD53B (right column) front-ends at 1 Grad.

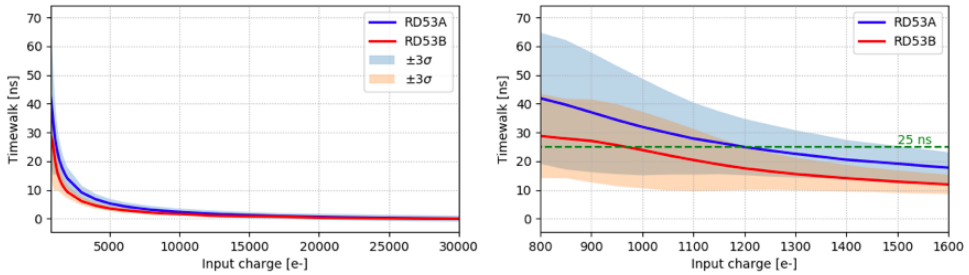

Figure 63: Time-walk at 1 Grad as a function of the input charge for RD53A (blue curve) and RD53B (red curve) FEs. The plot on the right hand side is a zoom of the time-walk for input charges ranging from 1100 to 1600 electrons.

for RD53A and 85 electrons for RD53B. It is worth noticing the large spikes for code=0 and 15 in the distribution of the TDAC codes for RD53A, pointing to a non-optimal behavior of the tuning DAC integrated in the RD53A version of the front-end.
Fig. 63 shows the time-walk as a function of the input charge for the two versions of the front-end. The plot on the right size is a zoom for input charges ranging from 800 to 1600 electrons. Notice, again, the significant smaller time-walk for the RD53B version, which

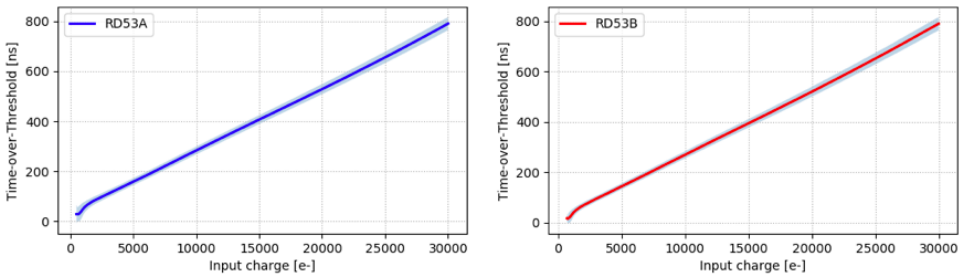

Figure 64: Time-over-Threshold as a function of the input charge for the RD53A (left plot) and the RD53B (right plot) front-ends.

confirms the improvement in time-walk already obtained in circuit simulations. Due to the different thresholds for RD53A and RD53B at 1 Grad, the maximum time-walk has to be evaluated for an input charge of 800 electrons for RD53A (around 42 ns) and at 900 electrons for RD53B (around 27 ns).

Fig. 64 shows the Time-over-Threshold as a function of the input charge for the RD53A (left plot) and the RD53B (right plot) front-ends. Both the front-ends have been biased in such a way to get, at room temperature, before irradiation, a ToT close to 133 ns for an input charge of 6000 electrons. A pretty linear behavior of the ToT has been obtained for both the versions of the front-end for input charges larger than 2000 electrons.

4.3 Chip3B: pre-rad results

Fig. 65 shows the tuned threshold (first row), noise (second row) and TDAC codes (third row) distributions for the RD53A front-end (left column) and the RD53B ones (right column). The target threshold for both RD53A and RD53B channels is close to 1100 electrons. Notice that the threshold dispersion for the RD53B version is around half the dispersion of the RD53A one. This is due to the additional trimming DAC bits integrated in the RD53B version, featuring a tuned-threshold dispersion close to 50 electrons. The tuned threshold dispersion obtained for Chip3B is larger than the one of Chip2 due to the larger value of LDAC_LIN (hence, the larger dyanmic TDAC range) used in Chip3B. The equivalent noise charge for both the versions of the front-end is slightly larger than 100 electrons, a value exceeding the ENC obtained for Chip2 due to the larger Krummenacher current used in Chip3B to reduce ToT.

Fig. 66 shows the time-walk as a function of the input charge for the two versions of the front-end. The plot on the right size is a zoom for input charges ranging from 1100 to 1600 electrons. Notice, also for Chip3B, the significant smaller time-walk for the RD53B version, which confirms the improvement in time-walk already obtained in circuit simulations. In

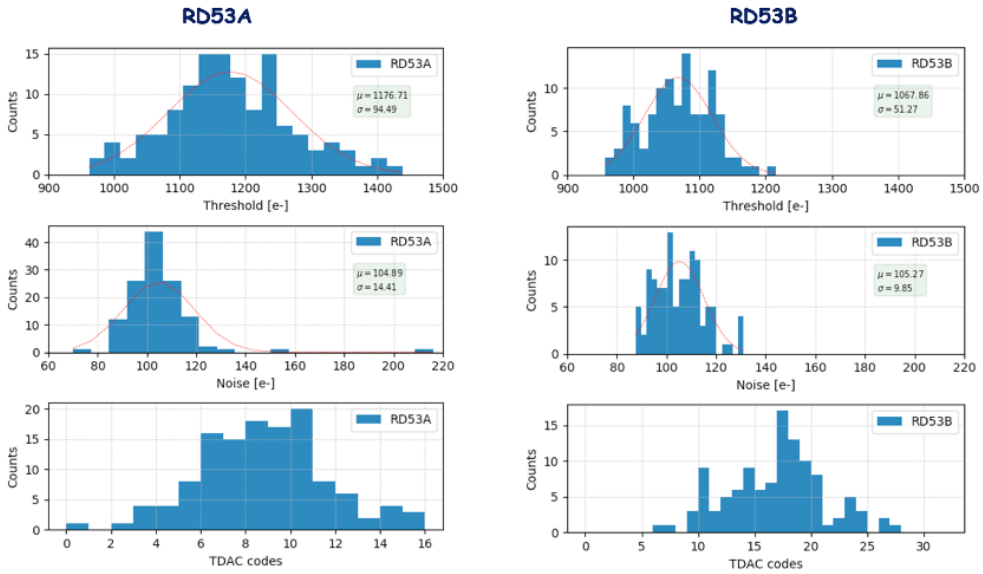

Figure 65: Threshold (first row), noise (second row) and TDAC codes (third row) distributions for the RD53A (left column) and RD53B (right column) front-ends.

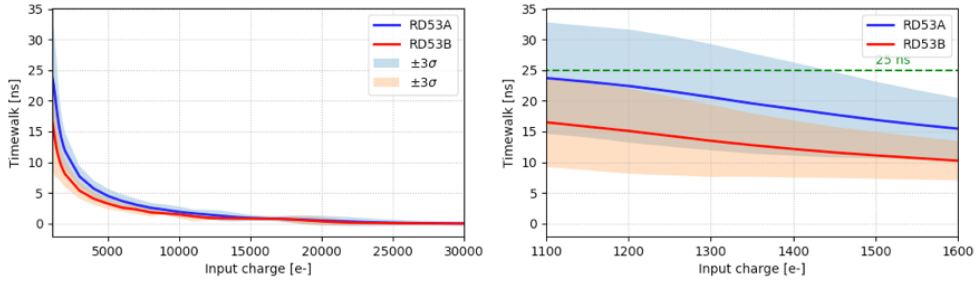

Figure 66: Time-walk as a function of the input charge for RD53A (blue curve) and RD53B (red curve) FEs. The plot on the right hand side is a zoom of the time-walk for input charges ranging from 1100 to 1600 electrons.

particular, a time-walk around 17 ns has been measured for the RD53B FE for an input charge close to the threshold, whereas a time-walk close to 24 ns has been detected for the RD53A version.

Fig. 67 shows the Time-over-Threshold as a function of the input charge for the RD53A (left plot) and the RD53B (right plot) front-ends. Both the front-ends have been biased in

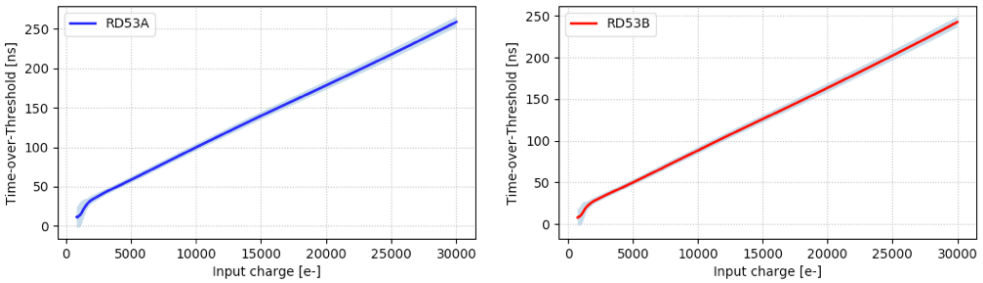

Figure 67: Time-over-Threshold as a function of the input charge for the RD53A (left plot) and the RD53B (right plot) front-ends.

such a way to get a ToT close to 70 ns for an input charge of 6000 electrons. The tuning of the preamplifier discharge rate has been performed at room temperature and has not been tweaked after cooling down to -10°C. A pretty linear behavior of the ToT has been obtained for both the versions of the front-end for input charges larger than 2000 electrons.

4.4 Chip3B: 1 Grad results

Fig. 68 shows the tuned threshold (first row), noise (second row) and TDAC codes (third row) distributions for the RD53A front-end (left column) and the RD53B ones (right column) after exposure to 1 Grad of X-rays. The mean threshold for RD53A and RD53B channels is close to 1100 and 900 electrons, respectively. Notice that the threshold dispersion for the RD53B version is significantly smaller than the one measured for RD53A. The equivalent noise charge, slightly larger with respect to pre-rad values, is close to 115 electrons for RD53A and 100 electrons for RD53B.
Fig. 69 shows the time-walk as a function of the input charge for the two versions of the front-end. The plot on the right size is a zoom for input charges ranging from 900 to 1600 electrons. Notice, again, the significant smaller time-walk for the RD53B version, which confirms the improvement in time-walk already obtained in circuit simulations. Due to the different thresholds for RD53A and RD53B at 1 Grad, the maximum time-walk has to be evaluated for an input charge of 1100 electrons for RD53A (around 28 ns) and at 900 electrons for RD53B (around 19 ns).

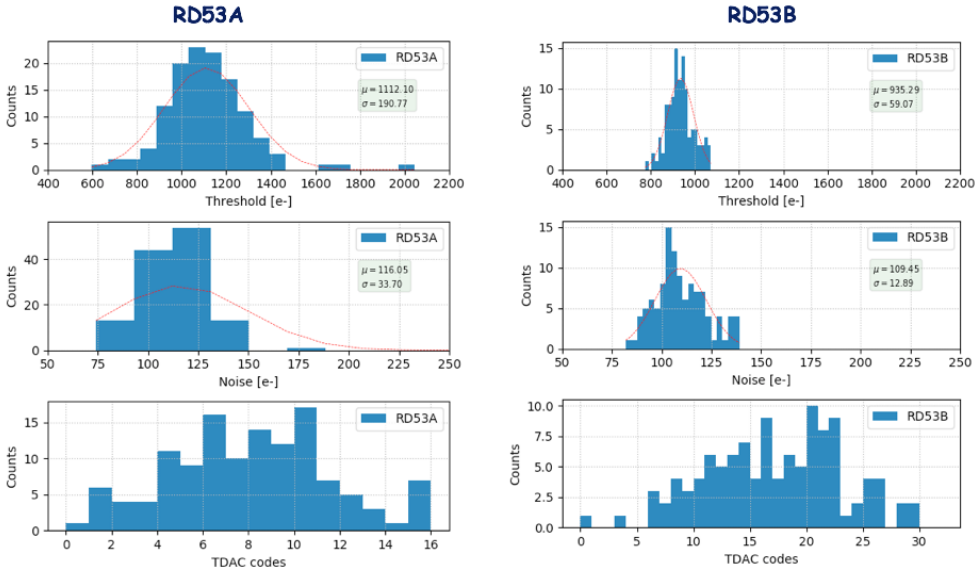

Figure 68: Threshold (first row), noise (second row) and TDAC codes (third row) distributions for the RD53A (left column) and RD53B (right column) front-ends at 1 Grad.

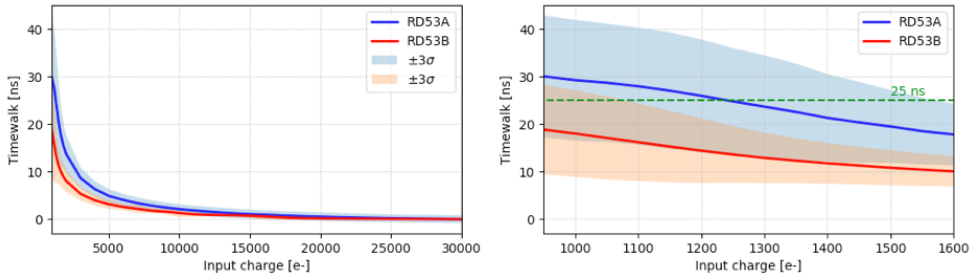

Figure 69: Time-walk at 1 Grad as a function of the input charge for RD53A (blue curve) and RD53B (red curve) FEs. The plot on the right hand side is a zoom of the time-walk for input charges ranging from 1100 to 1600 electrons.